

Suboptimal Estimator for the Spatial Orientation of a Pilot

by

Pierre E. Pommellet

Ancien Elève de l'Ecole Polytechnique, Promotion 1984

Ingénieur de l'Ecole Nationale Supérieure de l'Aéronautique et de l'Espace, Promotion 1989

SUBMITTED IN PARTIAL FULFILLMENT OF THE
REQUIREMENTS FOR THE DEGREE OF

Master of Science
in
Aeronautics and Astronautics
at the
Massachusetts Institute of Technology
September 1990

© Pierre E. Pommellet, 1990

The author hereby grants to M.I.T permission to reproduce and to
distribute copies of this thesis document in whole or in part.

Signature of Author _____

Department of Aeronautics and Astronautics

August 15, 1990

Certified by _____

Professor Lena Valavani

Thesis Supervisor, Department of Aeronautics and Astronautics

Accepted by _____

Professor Harold Y. Wachman

Chairman, Department Graduate Committee

MASSACHUSETTS INSTITUTE
OF TECHNOLOGY

SEP 19 1990

LIBRARIES

Aero

Suboptimal Estimator for the Spatial Orientation of a Pilot

by

PIERRE ERIC POMMELLET

Submitted to the
Department of Aeronautics and Astronautics
on August 10, 1990 in partial fulfillment of the requirements
for the degree of Master of Science in Aeronautics and Astronautics

Abstract

The Central Nervous System (CNS) uses sensory afferences to calculate an estimate of the orientation of the body in space. Considering that the process of spatial orientation tries to minimize the variance of the estimation error, with the assumption of knowing the dynamics of the internal sensors, it can be seen as an optimal observer (Kalman Filter).

An internal model of the spatial orientation is developed, using only vestibular cues. The angular velocities and linear acceleration are supposed to be the output of first order systems driven by white noise. The angular orientation is derived from the integration of a quaternion vector, which is part of the internal model. Since the system is nonlinear, the gain of the observer is calculated using suboptimal techniques (Extended Kalman Filter), under assumptions on the noise statistics.

The model predictions are compared with previous studies. The work in this thesis gives more accurate results and extends the range of applicability of the model. Sensitivity of the filter with respect to various parameters (frequency bandwidth of the expected signals, noise covariances) is studied. Finally the model is tested on real centrifuge cases.

Thesis Supervisor: Dr. Lena Valavani

Title: Associate Professor of Aeronautics and Astronautics

Acknowledgements

First of all, I would like to thank the Délégation Générale pour l'Armement of the French Government for having supported me here during this year.

Professor Lena Valavani, my thesis advisor has earned all my thanks for her advice and guidance throughout this study.

Thanks to the Man Vehicle Lab for giving me friends, office, advice and computer time.

And finally a special thanks to my wife Isabelle, who shared with me this year 1990, which has turned out to be full of emotion and adventure, which is still evolving, and is far from culmination.

Table of Contents

ABSTRACT.....	2
ACKNOWLEDGEMENTS	3
Chapter1 Introduction.....	6
1.1 General Considerations On Spatial Orientation.....	6
1.2 Thesis Organization.....	10
Chapter2 Sensors of the Orientation Process.....	11
2.1 Vision.....	11
2.1.1 Focal Vision.....	11
2.1.2 Ambient Vision	12
2.2 The Vestibular Function.....	13
2.2.1 The Semicircular Canals	14
2.2.2 The Otolith Organs	15
2.2.3 The Vestibular Reflexes.....	15
2.2.4 Voluntary Movement and Orientation Information	16
2.2.5 Thresholds of Vestibular Perception	17
2.3 Other Senses of Spatial Orientation	18
2.3.1 Non Vestibular Proprioceptor.....	18
Chapter3 Modeling of the Sensors.....	20
3.1 Coordinates Systems	20
3.2 Dynamics of the Sensors.....	21
3.2.1 The Semicircular Canals	22
3.2.2 The Otolith Organs	22
3.2.3 The Vision.....	23
3.2.4 Tactile and Proprioceptive Models.....	24
3.2.5 Proprioception Model	24
Chapter4 Internal Model and Suboptimal Estimator.....	26
4.1 Background.....	26
4.2 New Internal Model for the Central Nervous System	33
4.2.1 State Vector Propagation.....	35
4.2.2 Measurement Equations.....	38
4.3 Structure of the Central Nervous System	39
Chapter5 Implementation Considerations and Simulation	
Results	43
5.1 Time History Generation.....	43
5.2 Computer Implementation.....	45
5.2.1 Integration of the “Time History Generation”.....	45
5.2.2 Extended Kalman Filter.....	46
5.3 Simulation Results, comparison with previous studies.....	48
5.3.1 Yaw Motion	48
5.3.1.1 Rotation in the Light.....	49
5.3.1.2 Rotation in the Dark.....	50
5.3.1.3 Circular Vection	51
5.3.2 Forward Acceleration	51

5.3.2.1 Acceleration in the Dark.....	52
5.3.2.2 Acceleration in the Light.....	53
5.3.2.3 Linear Vection.....	55
5.3.3 Tilting Motion.....	56
5.4 Sensitivity to Filter Parameters.....	58
5.4.1 Frequency Bandwith in Angular Velocity.....	58
5.4.2 Frequency Bandwith in Linear Acceleration.....	59
5.4.3 Driving Noise.....	59
5.4.4 Measurement Noise.....	61
5.5 Centrifuge Experiment.....	62
5.5.1 Stimulus to the Vestibular System.....	64
5.5.2 Simulation Results.....	65
Chapter 6 Conclusions and Possible Improvements.....	69
6.1 Results Summary.....	69
6.2 Possible Improvements.....	69
References.....	71
Appendix A.....	74
A.1 Calculation of the Euler angles.....	74
Appendix B.....	76
B.1 Exemple of Quaternion Estimate.....	76
Appendix C.....	77
C.1 Main MatLab Code.....	77
C.2 Mechanism of a Simulation.....	89

Chapter 1

Introduction

1.1 General Considerations On Spatial Orientation

During the early ages of aviation, piloting a plane was nearly like riding a bicycle or sailing a boat, in the sense that there were very few instruments, and the control of stability and navigation in the air was left to the pilot's perception of orientation. In other words, piloting was accomplished with the view of the exterior world, the earing of the wind and the engine regime, and the basic sensations of movement that are provided by the whole body and, particularly, by the vestibular system.

When man wanted to fly in the clouds or at night or, in general, in "all weather" conditions, he had to invent a variety of instruments which allowed him to figure out the position in three dimensions of the aircraft by interpreting several measures. The modern pilot must now deal with a high workload environment and a complex instrument panel, without the possibility of hearing and, at times, without seeing the outside. He is, therefore, liable to introduce conflict between his internal feeling of orientation and the true orientation; this can result in "spatial disorientation".

Spatial disorientation has been recognized as a "silent killer" by the United States Air Force, being the cause of a noticeable number of crashes [1]. For example, if a pilot is distracted in total darkness by a warning signal or a radio problem, he is left to rely only on his senses to determine his orientation in space. A "cross check" of his instrumentation can correct the situation but, if it is misinterpreted or if the pilot doesn't do it for too long a time, and if the situation is critical (low altitude flight or very high speed), this can lead to a crash. Actually according to Freeman [1], spatial disorientation as a crash cause has been attributed to more

than 70 Class A mishaps in the Air Force since 1981. A Class A mishap is defined when the damage is over half a million dollars or if the pilot is killed.

According to Marlowe [2], we can classify spatial disorientation into three types. Type I, or “Unrecognized Spatial Disorientation”, is when the pilot is not aware that he is disoriented. This is particularly dangerous when flying in difficult situations and at very low altitudes. Type II is called “classic vertigo”. The pilot knows that he is disoriented and is able, in most of the cases, to cope with this sensory conflict and to manage the situation. Type III, or what is called “vestibulo-ocular disorganization”, occurs when the pilot is conscious of his disorientation but is totally unable to obtain correct orientation information. Because of the violence of the maneuver, the vision is blurred by counterproductive reflexes generated by the vestibular system. This kind of spatial disorientation is, however, quite rare.

In a study by Kirkham et al in 1978 [3], spatial disorientation represents 2.5% in the general aviation accidents in the U.S., and 7.11% and 6.75% for the Air Force and the Navy respectively. More recently [4,5], it has been shown that spatial disorientation was responsible for 14% of the USAF Class A mishaps, costing around \$ 1,000,000 and 5 to 10 fatalities per year. For 1988, 8 out of 57 accidents in the Air Force were actually due to spatial disorientation, and all of those but one were classified as Type I and occurred at night or in IMC (Instrument Condition). Those figures are not negligible at all and explain the interest that is given to a better understanding of the mechanism of the spatial orientation.

If we want to introduce, in a few words, what is the mechanism of the orientation in space, we will first focus on the role played by vision. When the pilot has a clear view of the horizon, ambient vision provides all the orientation information. But when the exterior vision is compromised, say by the clouds or the night, then the same motion that was well managed in clear weather can introduce disorientation, and the pilot then has to interpret and to trust his instrument panel in order to recover to a normal situation. We then see that the “vision dominance” of the orientation process falls into two types. Gillingham [6] calls them the “congenital type”, basically the orientation in clear weather, and the “acquired type” in which

the vision is focused on the instruments, and the information that is read is decoded through a procedure that has been learned by previous training. Vision is then able to dominate all other orientation cues like vestibular or proprioceptive sensations (vision dominance). However, the “acquired type” of vision dominance is not natural and, in absence of real orientation references,- and by real we mean related to our natural environment - the orientation system tends to give priority to other natural orientation cues. In other words, “artificial orientation” can be provided by diligent attention to the instrumentation, but the conflict can easily turn in favor of the vestibular information and introduce disorientation.

The orientation process can, therefore, be seen as the estimation of a state vector, in which included, among others, are the orientation angles and velocities [10]. The Central Nervous System then, uses the knowledge of the dynamics of the body and the sensors (model) as well as the values of the outputs of the different sensors (measurements) and their preferences, to minimize a kind of mean square error criterion and to find the best orientation vector that is consistent with the measurements. Such an optimal estimation process, in the linear case, is known as the Kalman Filter [11], which can be extended to nonlinear cases as well, under appropriate problem assumptions.

The general process of the orientation of a pilot can be described in terms of a block diagram by a model referred to as Oman's model [12,13], as shown in Figure 1.1. We give here the general form of that kind of processing, where the pilot reactions are included in the global loop of the motion. What we call "Body and Exterior Dynamics" represents the movement in the inertial space, given a set of exterior conditions (airplane dynamics, pilot dynamics, control commands and so on). The output of that block is the actual value of a state vector containing all the information required to describe the spatial orientation. A measurement of that state vector is then used to calculate an orientation estimate, using a classic form of observer theory (the input to the observer being the difference between the actual measurement and the reconstruction of the measurement from the estimated value). Finally, the control strategy is calculated from the value of the estimate.

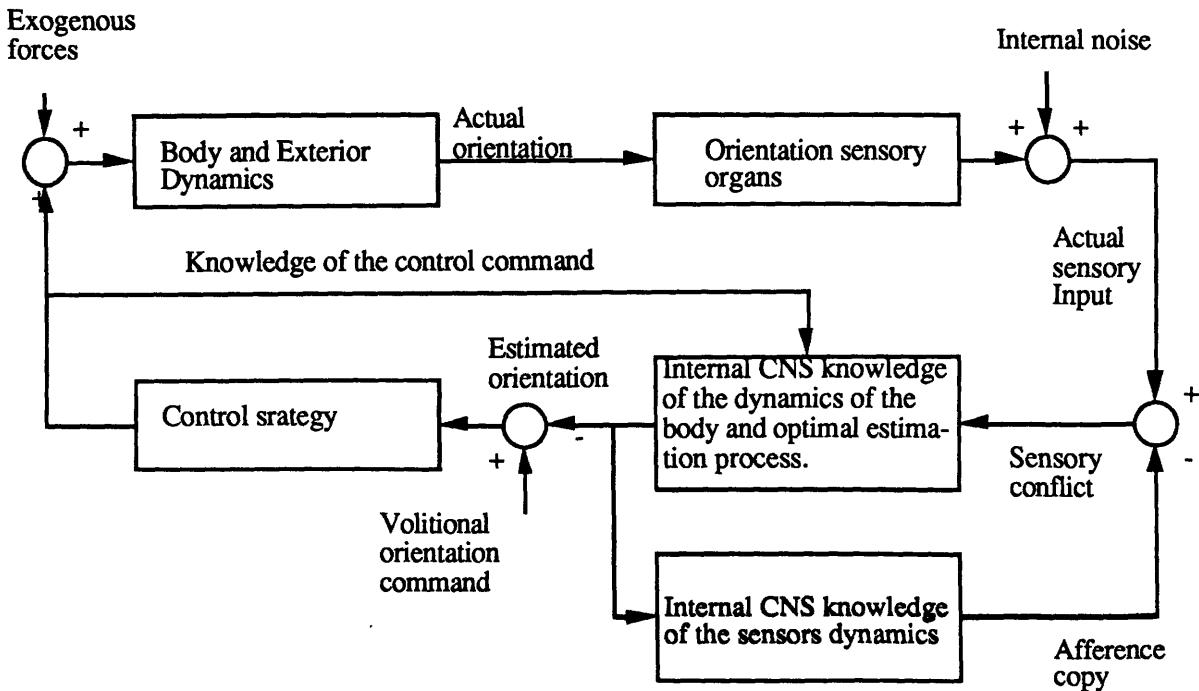


Figure 1.1: Oman's Model for the Orientation Process

The model set up by Borah et al [10] is essentially Oman's model, without the control part. In other words, they considered, for instance, the case of a passenger in an aircraft, or the case of a human who is not responsible for his movement in space. They also simplified the internal model of the CNS, using linearization about an upright position of the head in a 1 g environment, and employed a steady state optimal estimator (steady state Kalman filter).

In his PhD thesis, Dan Merfeld [16] also developed a model for the spatial orientation of the squirrel monkey, and ended up with the same kind of observer, with a constant gain chosen to best match experimental results. However, one of the main issues of Dan Merfeld's work was to introduce nonlinearity in the internal model in order to demonstrate that the CNS was trying to keep track of the orientation of the gravity vector. What we want to do here is to generalize these approaches, in order to come up with a more general model, which need not

be linear and which uses suboptimal filtering techniques in order to calculate a time varying gain. This generalization would lead to a wider coverage of the phenomena and expanded model applicability.

1.2 Thesis Organization

In Chapter 2, “Sensors of the Orientation Process”, we describe in detail the mechanism of the principal sensors of the orientation process, which are the visual and the vestibular systems. We also list other orientation sensors such as the proprioceptive and the auditory systems which appear to have some importance.

In Chapter 3, “Modeling of the Sensors”, we describe the quantification, in terms of transfer functions and nonlinear functions, of the input-output relationships in the different sensors.

In Chapter 4, “Internal Model Optimal Estimation Process”, we give the structure of the central process in terms of optimal estimation and the time-varying Kalman Filter.

Before concluding, we give in Chapter 5, “Implementation Consideration and Simulation Results”, the prediction of our model in basic simulations corresponding to experimental cases such as rotations and linear accelerations in the light or in the dark. The simulations were done using Borah et al [10] data, in order to compare the two approaches.

Chapter 2

Sensors of the Orientation Process

2.1 Vision

Vision is by far the most important sensor of spatial orientation and, for the most part, its function is obvious. One sees where one is and how one is moving and, therefore, knows where one was and where one is going to be. However, as we mentioned before, we can separate the visual orientation process into two distinct categories with two distinct functions: The focal vision that can be relied upon for object recognition and information interpretation, and the ambient vision or general spatial orientation.

2.1.1 Focal Vision

Following the description of Liebowitz and Dichgans [7], the focal vision is concerned with object recognition and identification, involving very fine details or high frequency signals. In other words, the focal vision gives material to the central processor in order to answer the “what” question.

Although focal vision is not directly related to orientation, it is the way information is read from the instruments and, therefore, provided one has instrument flying skills, those readings can be transformed into orientation information.

Also, in a visual flight environment, focal vision provides the basic cues from which appreciation of distance and depth are made. Actually, interpreting the change in the shape of the objects that appear in the visual field, or interpreting the motion parallax (the relative speed of the different objects that are seen) provides useful orientation information. Other cues, such as perspective or accommodation of the eye lens are also used but are of less importance.

2.1.2 Ambient Vision

Liebowitz and Dichgans [7] describe it as the way of subservient spatial orientation and answering the “where” question. Unlike focal vision, it is not systematically related to optical image quality and uses somewhat low frequency visual information. The fact that this ambient vision can be completely uncorrelated from the focal vision is experienced everyday by each of us when reading, while walking or driving for example. The vision is focused on the book or the newspaper, but we can still walk or drive properly.

The function of the ambient vision in the orientation process is double, providing both motion cues and position cues. Whether it is angular or linear, the perception of a moving background results in a perception of self-motion calledvection (angular vection or linear vection). Again, almost everybody has experienced the strong sensation of movement when looking at a moving train while being seated in another train parked next to it. Also, the wide screen motion pictures are using this effect to give a sensation of motion that can really be amazing. The position cues are used for the stabilization of the posture. They are also the cause of height vertigo, which is nothing more than a sensory conflict between the visual system and the vestibular system, due to erroneous information given by the ambient vision.

Another way of perceiving the distinction between ambient and focal vision is to say that focal vision serves to orient an object relative to oneself, whereas ambient vision serves to orient oneself relative to the perceived environment. As their functions are complementary, both focal and ambient vision are necessary to give adequate information of orientation in space.

Finally, to conclude this small section on the description of visual orientation, let us say a word about the eye movements. Actually, and this is particularly true in the case of the focal vision, the image of the perceived object needs to be stabilized in the retinal plane which is done by combined movements of the eyes and the head. These actions can either have the form of a slow pursuit (basically for a target going less than 60 deg/s) or some rapid and saccadic movements triggered voluntarily or reflexively, involving both the head and the eyes.

2.2 The Vestibular Function

The vestibular system is the second most important sensor of the spatial orientation process. This is for three reasons. First, it gives the substrate for the reflexes that serve to stabilize the vision when the head or the body are moving. Second, it provides some orientation information which is processed by the central nervous system in order to activate both skilled and reflexive motor activities. Third, in absence of vision, the vestibular system provides an accurate perception of motion as long as the maneuvers are in the range of what is naturally occurring.

We will not describe here the anatomy of the vestibular system; the interested reader is referred for that to Gillingham and Wolfe (6). However, Figure 2.1 presents its basic anatomy.

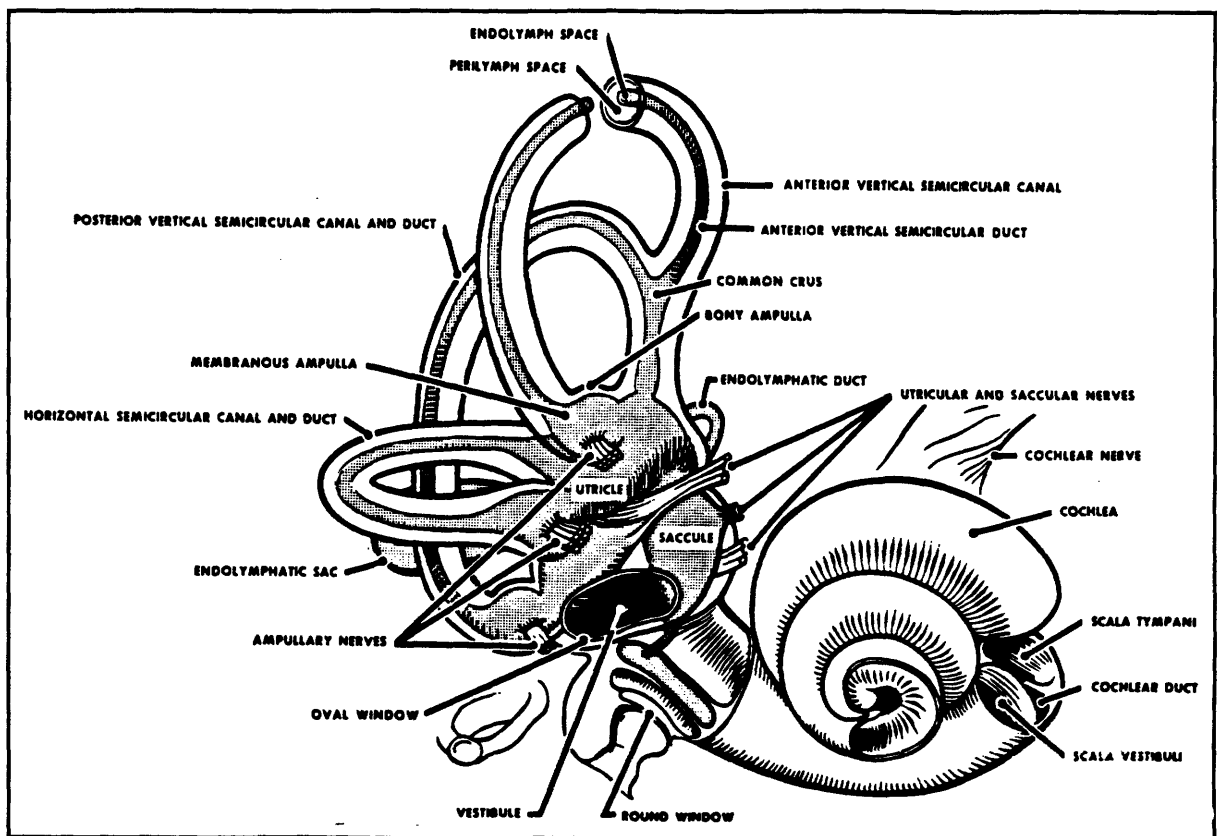


Figure 2.1 The Vestibular System (from Gillingham and Wolfe, 1987)

This small organ measures no more than 1.5 cm (0.6 inches) across, and it fits in the petrous portion of the temporal bone. The bony semicircular canals and vestibule contain the membranous semicircular ducts and otolith organs. What we are more interested in here is, of course, the function of that vestibular system and how the information is processed by its two major components, which are the semicircular canals and the otolith organs.

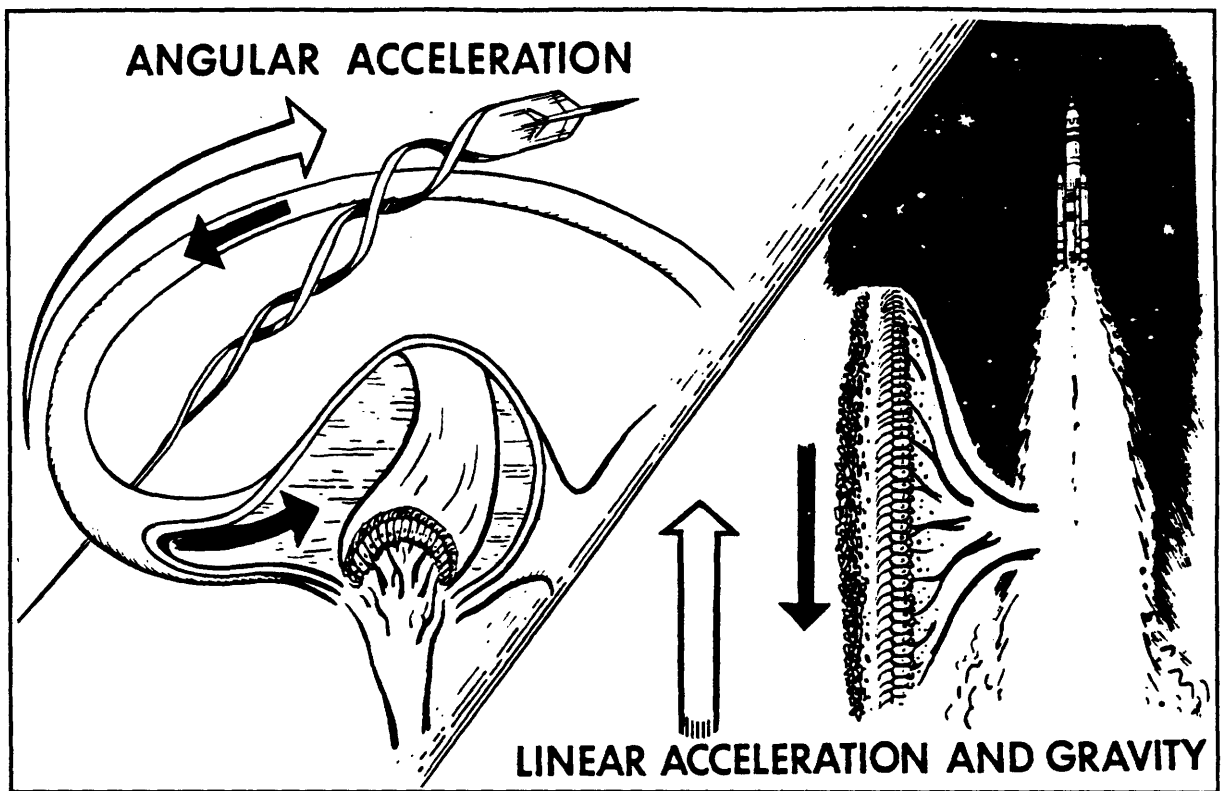


Figure 2.2: (from Gillingham & Wolfe, 1987)

2.2.1 The Semicircular Canals

The semicircular canals are fluid-filled rings that respond to angular acceleration providing a component of the three-dimensional rotation vector, normal to the plane of the ring, acting, therefore, as approximate integrators. As a result of their arrangement, the three planes of the three canals are almost orthogonal, and can detect an angular acceleration around any axis in space.

2.2.2 The Otolith Organs

The otolith organs act like linear accelerometers. Like the semicircular canals, they are able to detect an acceleration in three dimensions and, therefore, are the principal nonvisual determinants of the local vertical. However, due to the indetermination principle (which is one of the results of General Relativity), no instrument is able to distinguish between the gravitational acceleration and the total acceleration. Therefore, the otolith organs give only a value of the specific force (basically the gravity minus the total acceleration) that is applied to the body.

The functions of the vestibular system are basically the vestibular reflexes, the voluntary movements and the perception of orientation that we are going to describe in the next subsection of this chapter.

2.2.3 The Vestibular Reflexes

As we stated before, the retinal image is mainly stabilized by reflexes having vestibular origin, or Vestibulo-Ocular Reflexes (VOR). Basically, as shown in Figure 2.3, an angular acceleration is detected by the semicircular canals which trigger the activation of the muscles of the eyes in the opposite direction. Other VOR's are originated by the otolith organs, the movement of the eyes responding to a linear acceleration.

Those reflexes are very important in understanding the input-output relationship of the vestibular system. Actually, as the movement of the eyes is quite easily measurable, whether by implanting sensor devices by surgery on animals [16] or simply by using video images of the eye during the experiment, the VOR reflects the response of the vestibular system to a determined input. Most of the experiments done on the subject use that fact to determine the mathematical models that describe the vestibular function, which we are going to use throughout this study.

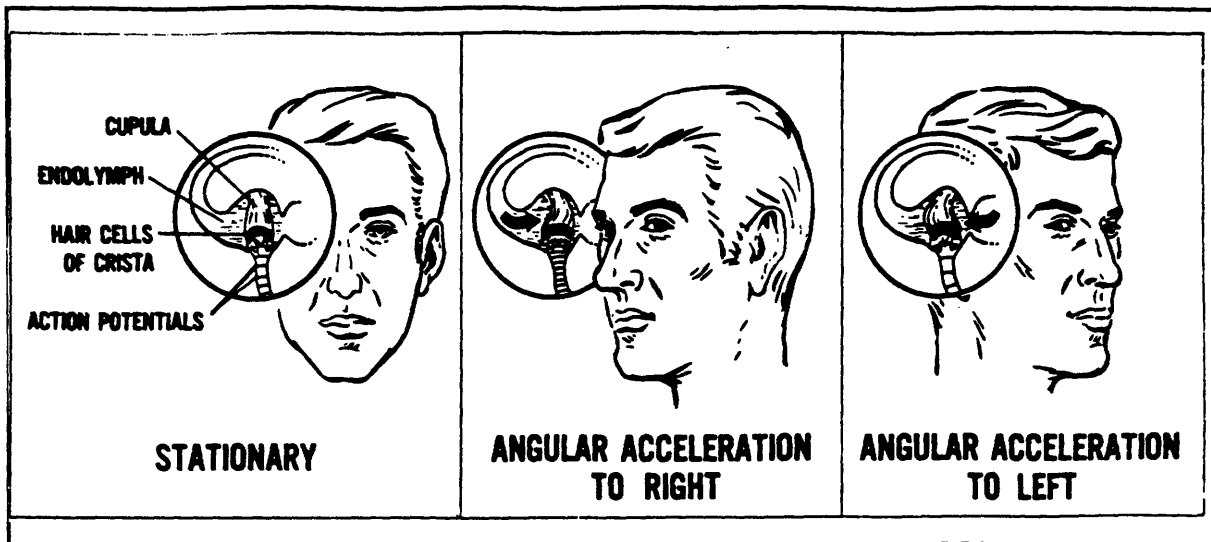


Figure 2.3 Vestibulo Ocular Reflex

Reflexes such as vestibulocollic reflexes (movement of the neck and the head in response to vestibular stimulation), or vestibulospinal reflexes (rapid activation of various muscles in response to a falling sensation, or in the maintenance of the upright posture for example), are other expressions of the vestibular function, but our understanding is less developed because of experimental difficulty in studying them.

2.2.4 Voluntary Movement and Orientation Information

The vestibular information not only serves to stabilize the body and the retinal image, but also provides data for the proper execution of voluntary movements. The skilled movements that we execute every day, when writing, riding a bicycle or playing an instrument for example, are most of the time done in "open loop", in the sense that we don't necessarily need some feedback information to execute them properly. The violinist doesn't have to look at his or her fingers while playing, or we can write a signature without looking at it. But the correct execution of such an automatic sequence in a specific environment necessitates a spatial orientation notion, provided by the process of all the outputs of the different sensors of our

body. In other words, when doing a skilled movement, whatever the position in space, we decide what we want the output to be, and initiate the command to do it and let the sequence run. Our body takes care of the details, using stored programs and the current preconscious orientation perception.

2.2.5 Thresholds of Vestibular Perception

One must be aware that orientation illusions can appear from the fact that thresholds are present in all those natural sensors. Even if they are difficult to measure, due to the fact that when the motions are close to the thresholds values the subject is more willing to say "maybe" than "yes" or "no", a great deal of work has been done on that subject, providing usable results.

Reasonable values for the perception of angular velocity by the vestibular system are 1.58 deg/s, 2.04 deg/s and 2.07 deg/s for yaw, roll and pitch motions respectively [8].

For the otolith organs, a 1.5 deg. change in the direction of g is perceived under ideal conditions. The minimum perceived linear acceleration was reported to be between 0.001g and 0.03g, but values of 0.01g for a_z and 0.006g for a_x and a_y seem to be appropriate [6].

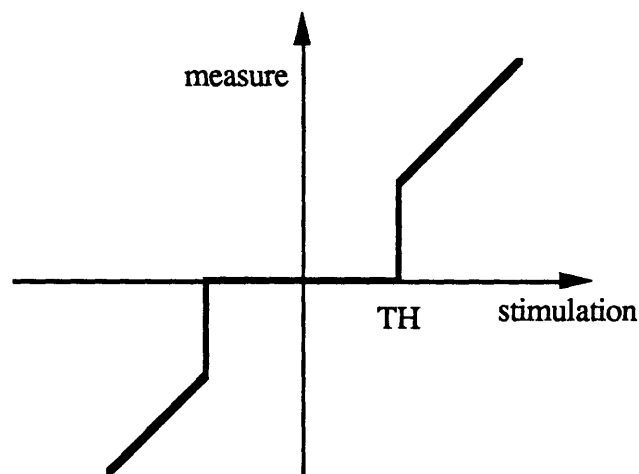


Figure 2.4 Input-output relationship of a threshold

2.3 Other Senses of Spatial Orientation

Although visual and vestibular cues are the main information used by the central processor in order to determine the spatial orientation, it turns out that other senses are not to be ignored. Especially important are the nonvestibular proprioceptors (muscles, tendon and joint receptors) and the cutaneous exteroceptors. However, it has been shown that, if a person is lacking one of the main orientation sensors, vision or vestibular system, he is able to maintain equilibrium and to move properly using the remaining sensor. But if both vestibular and visual systems are lost, then the postural stability and the natural locomotion are not possible any more.

2.3.1 Non Vestibular Proprioceptor

Muscles and tendons contain complex sensory end organs, which are the basis for some basic reflexes of the natural position and locomotion. By that fact, the reaction of such organs to the exterior environment, as for example the control of the position of the head during maneuvers involving linear accelerations, gives to the central processor information about the total acceleration of the body.

The joints which are present in our articulations are also recognized to be sensory perceptors. The perception of the motion by those joints reaches consciousness, with sometimes a low threshold, as low as 0.5 deg when moved at greater speed than 1.0 deg/s (6).

By being able to perceive touch, pressure, heat and cold, the cutaneous exteroceptors can also be used to contribute to spatial orientation.

Finally, last but not least, are the auditory cues. By allowing us to determine at the surface of the earth the direction of a sound source, auditory information can play a major role in our orientation process. Also, even if the noise level is very high in an aircraft, a pilot can use his auditory sensors to recognize an engine regime or the frequency of the air passing by the cockpit and transform that into orientation information, such as incidence or airspeed.

Very recently [9], experiments have been conducted to measure the efficiency of providing additional auditory cues to a pilot, in order to improve recovering from spatial disorientation. It turned out that the results were good for at least small and medium angles.

After describing the different sensors of the spatial orientation, we are now going to show their mechanism in term of transfer functions and nonlinear functions (such as thresholds) relating the input, or the exterior stimulations, and the output, or which information is received by the central processor. This is done in the next chapter.

Chapter 3

Modeling of the Sensors

3.1 Coordinates Systems

The Earth is considered to be inertially stable, which is justified by the small amplitude of the dynamics that we are considering in space-time. Therefore let us consider an (XYZ) coordinate system related to the Earth, and an (x,y,z) related to the vehicle in which the pilot is flying, Figure 3.1.

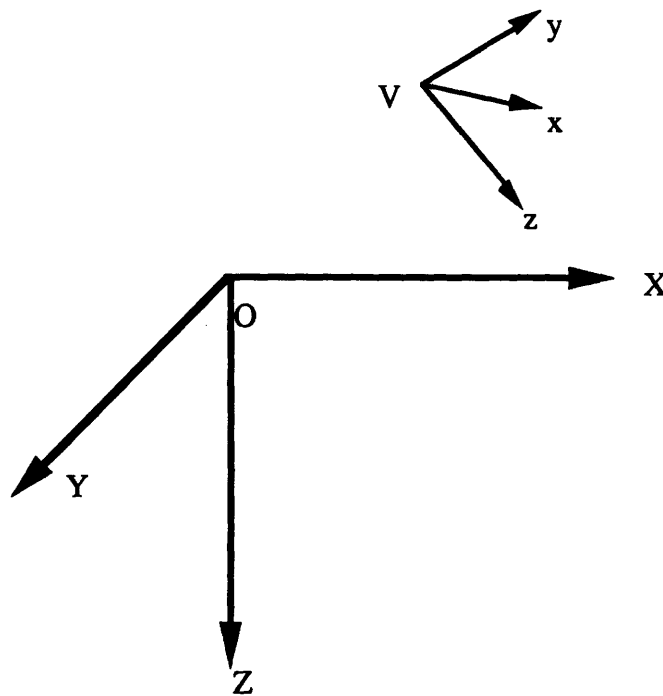


Figure 3.1 Coordinate systems

We can then define (x_{hd}, y_{hd}, z_{hd}) related to the head of the pilot, (x_c, y_c, z_c) characterizing the input axes of the semicircular canals, and (x_o, y_o, z_o) for the otoliths as shown in Figure 3.2. Note that, for modeling purposes, we are considering a cyclopic set of canals and otoliths situated at the center of the head.

An input to our sensors model can therefore be characterized by a function of time describing the movement of (V,x,y,z) in the inertial space. The orientation process then, consists of knowing at each time the transformation matrix between (x,y,z) and (X,Y,Z) , or $B(t)$.

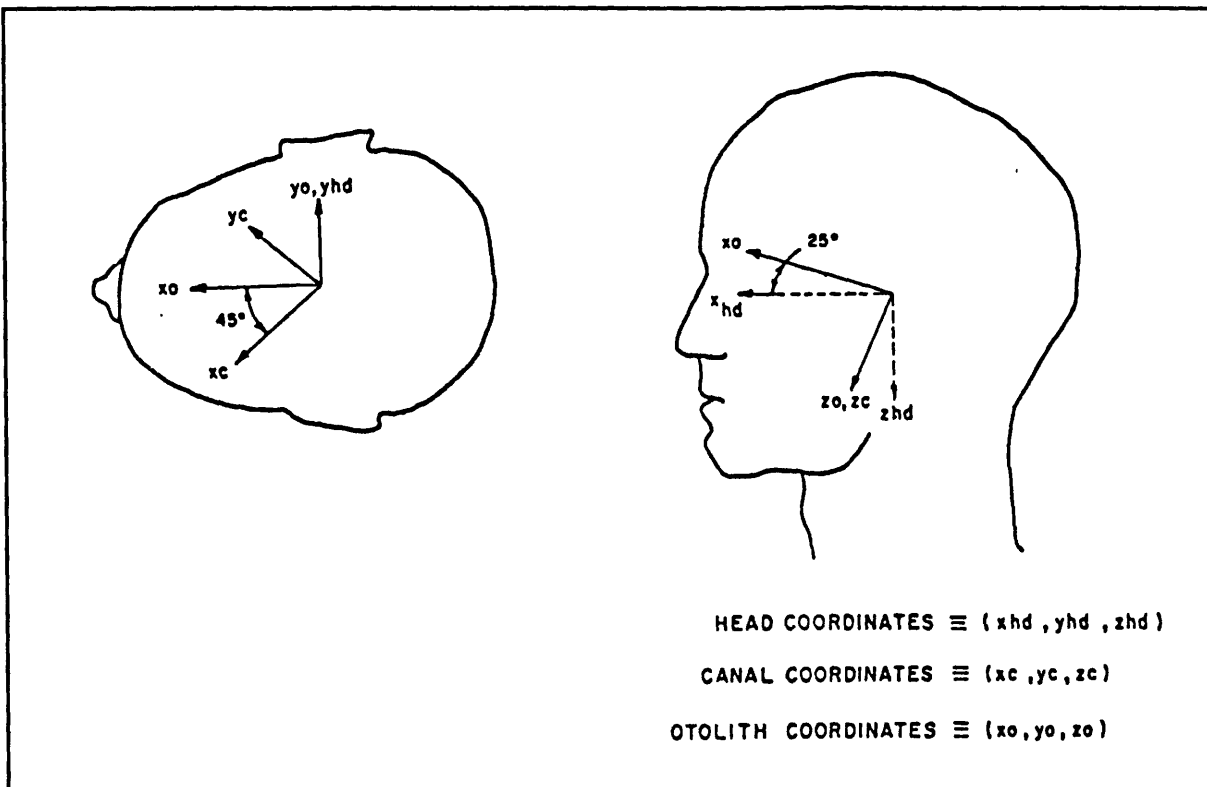


Figure 3.2 Cyclopan Sensor Coordinates

3.2 Dynamics of the Sensors

In the following paragraphs we are going to give the transfer functions that represent the input-output relationships of the different sensors previously described. The numerical values have been found experimentally and usually differ from one author to another. The data used in Borah et al [10] seem to be quite far from what is believed to be acceptable values for the time constants of the different dynamics. Our main reference is then going to be Dan Merfeld's PhD

Thesis [16] for the semicircular canals and the paper by Grant and Best [21] for the otoliths. However, we have to be aware that while the modelization of the semicircular canals is quite well accepted, the same is not true for the otolith organs.

3.2.1 The Semicircular Canals

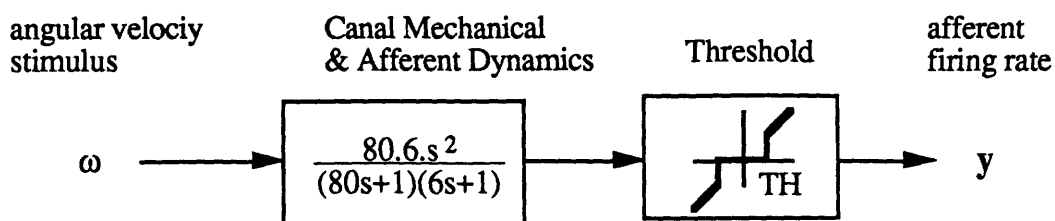


Figure 3.3: Semicircular Canal Model

Figure 3.3 shows the dynamics represented by a second order filter with two time constants at 6 and 80 seconds, followed by a threshold function. The stimulus is, of course, three-dimensional and each component of the acceleration is processed in the same way, with only a change in the value of TH (the threshold value). The components of the vectors γ and y are given in the coordinate system related to the canals.

3.2.2 The Otolith Organs

As said previously, the modeling of the otolith organ dynamics is not as well investigated. A mathematical model of a small mass which responds to linear acceleration would lead to a second order dynamics with two time constants. A 10 second value for the slow time constant seems to be appropriate. The short time constant, on the other hand, is subject to disagreements among different authors. Recently, in a paper on that topic, Grant and Best [21] came up with a value of .0002 seconds for the short time constant. However, for implementation considerations, because of the nonlinearities that we are going to consider and,

in order to make numerical simulations possible with a reasonable time-step, we will use here a value of .01 for the fast dynamics.

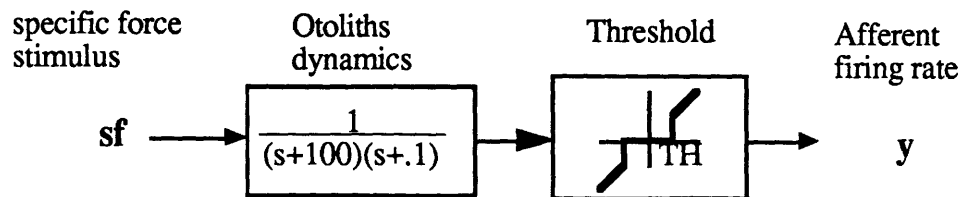


Figure 3.4: Otolith Model

As we did for the canals model, the components of the specific force vector and the corresponding afferent response are given in the coordinate system related to the otoliths.

3.3.3 The Vision

We saw that the vision was giving a very good estimate of the general orientation of the body, by what we called either “ambient vision” or “focal vision”. Also, due tovection phenomena, whether linear or angular, a moving visual field induces a sensation of self-movement roughly proportional to the velocity of the background field up to a saturation level of about 60 deg/s and 5m/s respectively [15]. The dynamics of the visual sensor can, therefore, be modeled by unity. However, in the case of the focal vision, the pilot is interpreting the orientation vector from the reading of the instruments, and this can take a certain amount of time when trying to recover from a spatial disorientation situation. We can, therefore, separate the vision in two branches: The ambient vision with unity dynamics and a saturation level for the measurements of the velocities, and the focal vision with an $\exp(-ts)$ (delay of τ) dynamics.

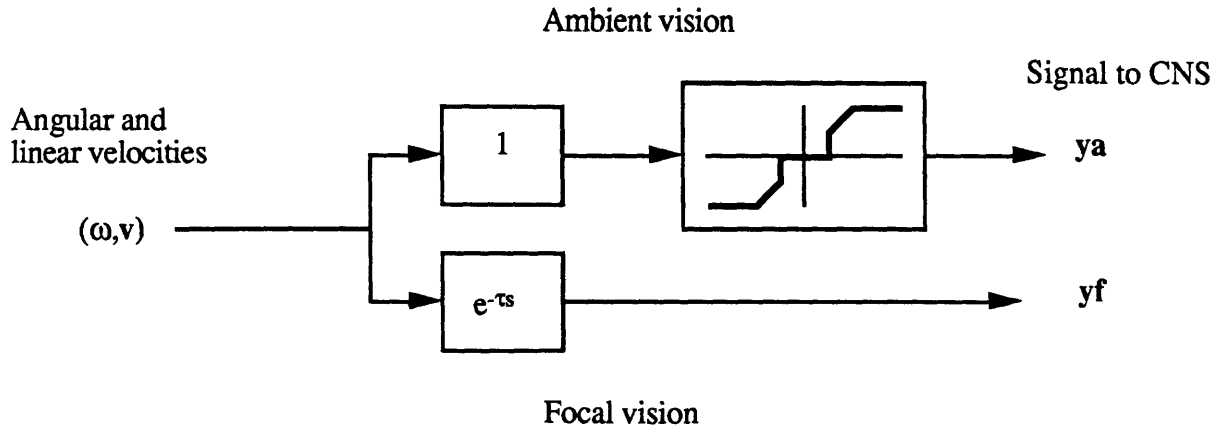


Figure 3.5: Vision Model

3.3.4 Tactile and Proprioceptive Models

Obviously, the body is able to perceive information about the direction and the intensity of the specific force when it is subjected to acceleration by the feeling of pressure exerted by the seat. Although it is not well documented in the literature, Borah et al [10] use a simple lead-lag transfer function to represent the characteristics of the major mechano-receptors.

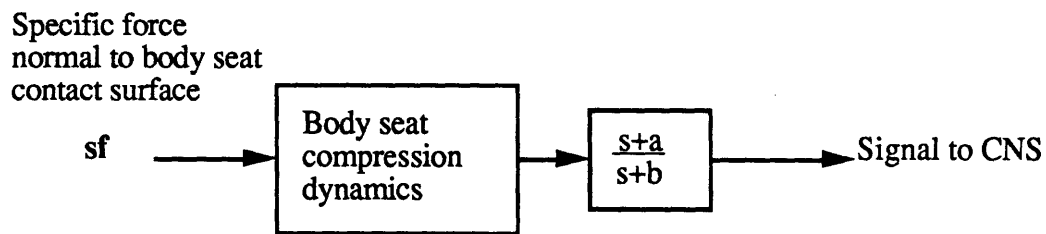


Figure 3.6: Tactile Model

The value used by Borah et al are $1/b=10$ msec and $a/b=1/10$.

3.3.5 Proprioception Model

Although the main part of the body is buckled in the seat, the head-neck system is almost free (at least on a lateral axis) and can be thought of as an inverted pendulum whose position is

maintained by the action of several muscles of the neck. Therefore, the reaction of those muscles to certain specific forces provides very strong information about the exterior environment and spatial orientation. Gum [17] modeled that system as a classic inverted pendulum compensated by first order compensators.

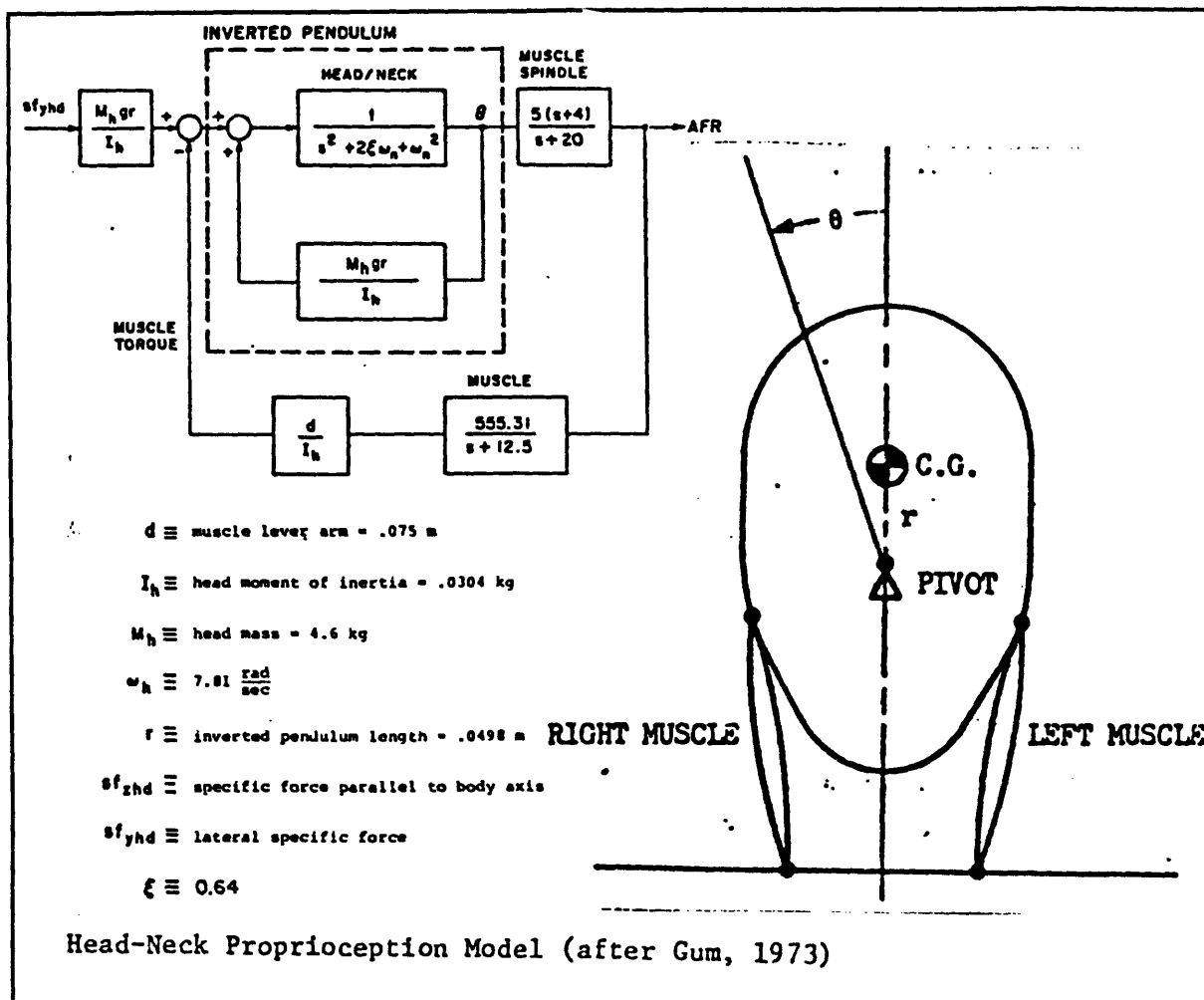


Figure 3.7: Proprioceptive model

However, the addition of tactile and proprioceptive cues as modeled in Borah et al. [10] had turned out to give very limited results while it increased the complexity of the model by adding four states to the state vector. Hence, it didn't seem necessary to include those in our model.

Chapter 4

Internal Model and Sub-optimal Estimator

4.1 Background

Since the early fifties, scientists started to become interested in setting up mathematical models to represent the mechanism of the CNS. In Dan Merfeld's thesis [16], an entire paragraph refers to the history of those models, which are often referred to as Von Holst's, Held's, Reason's or Robinson's models.

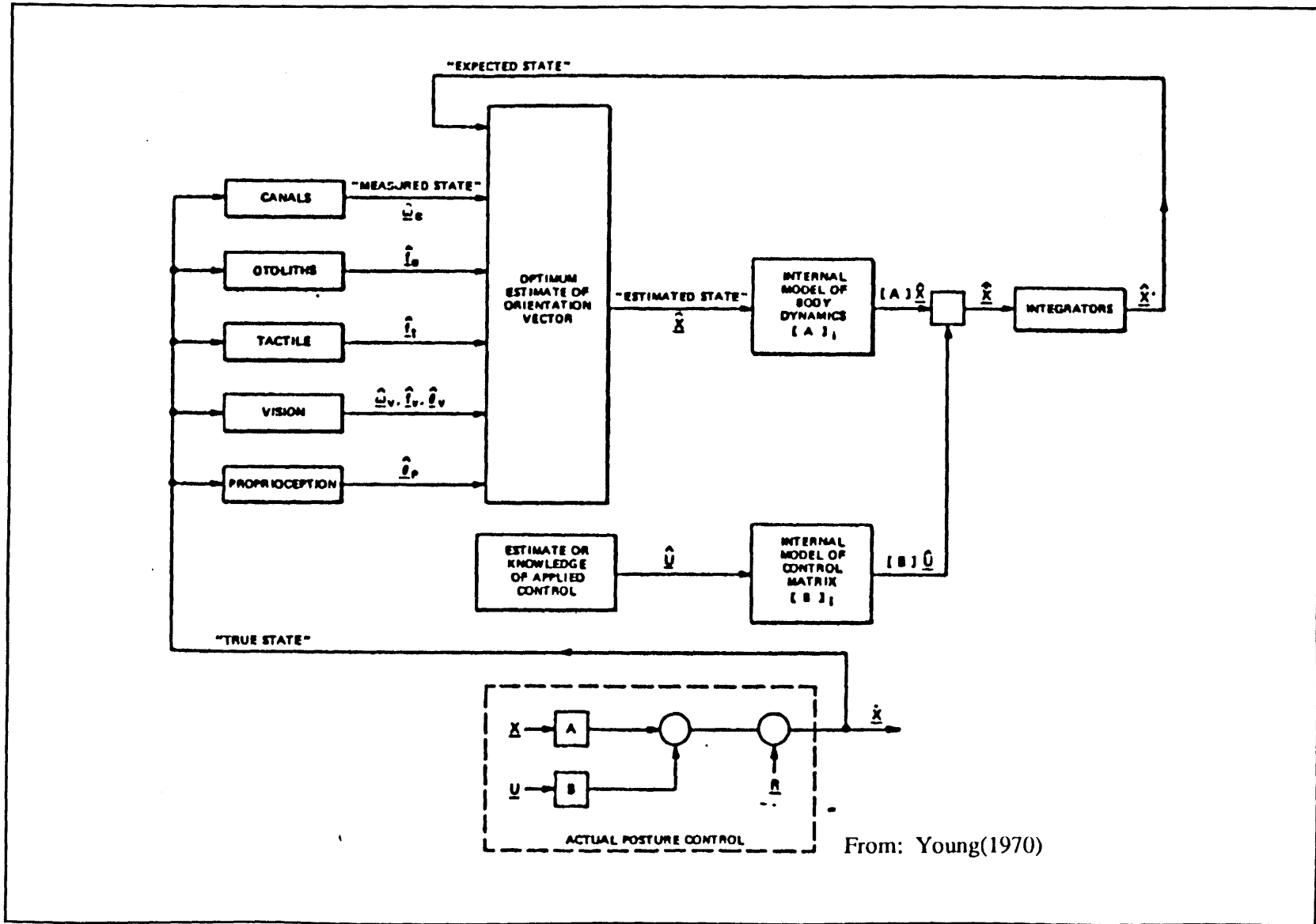
As mentioned previously, the bottom line of that study is the use of optimal estimation techniques, developed since the late sixties, by people like Young [18], Borah [10] or Oman[12].

In 1970, L. Young [18] came up with the idea that spatial orientation might be expressed as an optimal estimation problem, the CNS using the output of the natural sensor to update an estimate of a state vector of the spatial orientation, as in Figure 4.1.

The model used by Borah, Young and Curry [10] in their investigation of spatial orientation was exactly the same as that in Figure 4.1. This model can be divided into two parts. First, a "time history generation", or the calculation of the output of the different sensors for a specific motion. Second, the optimal "mixing" itself, with the calculation of the gain and the estimate update.

The "true state" of the model is a vector containing the major "spatial orientation" information such as the angular velocity, the orientation angles, the linear velocities and accelerations, and all the internal states coming from the representation in state-space of the transfer functions of the different sensors. The different dynamics of the internal sensors provide then a measurement of that "true state", or "measured state".

YOUNG'S MODEL



From: Young(1970)

Figure 4.1

If we represent the evolution of the "true state" by a differential equation of the form:

$$\dot{x}=f(x,u,t)$$

where f is a regular function, and if the measurement is represented by:

$$z=h(x)+\theta$$

where h , has the same regularity as f and where θ is a measurement noise, then the mechanism of the orientation process can be written as:

$$\hat{\dot{x}}=\hat{f}(\hat{x},u,t)+K(z-\hat{h}(\hat{x},t))$$

where the hatted expressions represent the internal estimation of the state vector, and the internal representation of the dynamic function and the measurement function (or the internal model). In other words, the CNS has an internal representation of the dynamics involved, and uses it to calculate the gain of the estimator.

Borah et al [10] consider the case of a passive subject, having no a-priori information about the angular velocities and linear acceleration that are going to be applied. However, they do consider that the subject is expecting those signals in a certain frequency bandwidth, as shown in Figure 4.2.

Using a linearization about an upright head position, the angular velocity is integrated to give the orientation angles. The specific force is then calculated as the difference between the rotated gravity and the linear acceleration. The angular acceleration and the specific force are then the inputs of the transfer functions of the eye-vestibular system sensors, to create an expected measurement. It is also assumed that the CNS has perfect knowledge of the different dynamics and measurement functions.

This linearized internal model can therefore be written as:

$$\dot{x}=Ax+\xi$$

$$z=Cx+\theta$$

x being a (25X1) state vector and z a (12X1) measurement vector, with θ and ξ white noises with predetermined intensity (covariance matrices R and Q respectively).

INTERNAL MODEL OF YOUNG'S MODEL

From Borah et al [10]

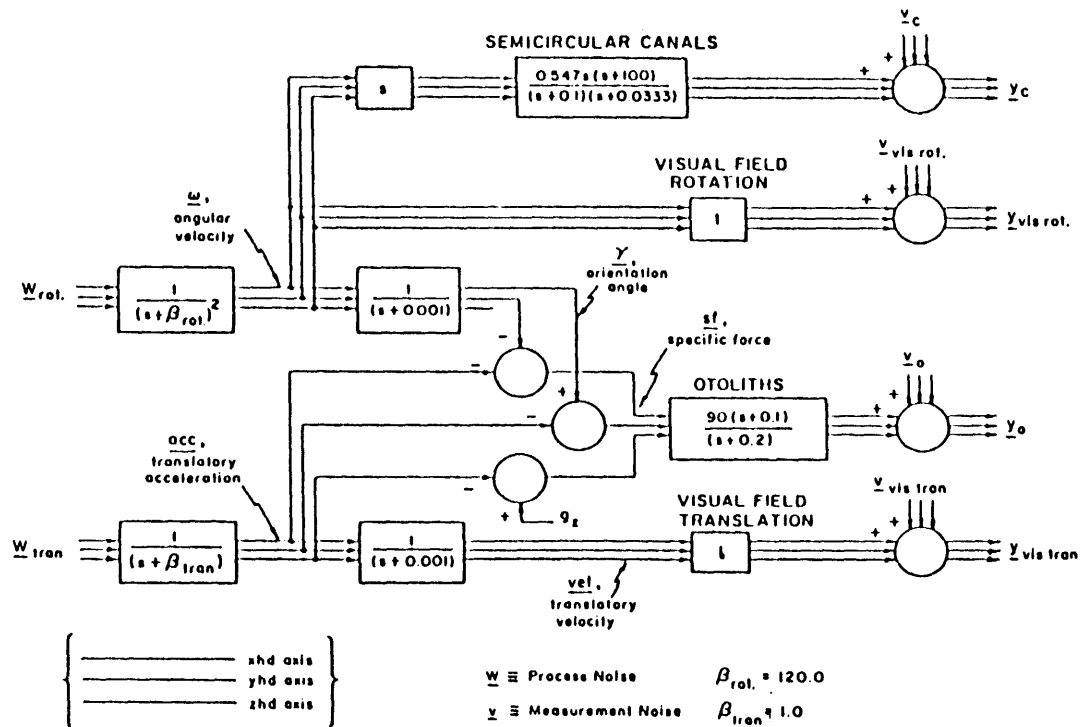


FIGURE 7. Internal model for visual vestibular interaction. The coordinate frame is the "head axis" system defined in FIGURE 1. The internal model is linearized about a head-upright, 1-g environment and assumes the visual field to be inertially stable. Integrators are approximated by low pass filters with long time constants ($\tau = 1000$ seconds) to avoid the computational difficulties that would otherwise be caused by infinite state covariance values. The process and measurement noise intensities used are specified in the APPENDIX.

The internal estimate is calculated by a classic Kalman Filter, assuming initial condition on the estimate and on the estimation error.

$$\begin{aligned}\hat{\mathbf{x}} &= \mathbf{A}\hat{\mathbf{x}} + \mathbf{K}(z - \mathbf{C}\hat{\mathbf{x}}) \\ \mathbf{K} &= \mathbf{P}\mathbf{H}^T\mathbf{R}^{-1} \\ \dot{\mathbf{P}} &= \mathbf{A}\mathbf{P} + \mathbf{P}\mathbf{A}^T + \mathbf{Q} - \mathbf{P}\mathbf{H}^T\mathbf{R}^{-1}\mathbf{H}\mathbf{P}\end{aligned}$$

For simplicity, Borah et al are using a steady state version of the Kalman Filter, taking the steady state value of the covariance of the estimation error from the solution of the Filter Algebraic Ricatti Equation:

$$0 = \mathbf{A}\mathbf{P} + \mathbf{P}\mathbf{A}^T + \mathbf{Q} - \mathbf{P}\mathbf{H}^T\mathbf{R}^{-1}\mathbf{H}\mathbf{P}$$

According to Borah et al, the predictions of their model were matching experimental results from several authors pretty well. They were also able to represent some of the phenomena experienced in motion, such asvection or tilt perception during linear accelerations.

However, the linearization around the upright head position implies that the orientation angles must remain very small in the internal model. This point must now be reconsidered in light of recent studies. Actually, one of the issues in Dan Merfeld's thesis was to prove, at least in the case of the squirrel monkey, that the CNS was keeping track of the orientation angles and of the "down" direction in particular. In other words, a model for spatial orientation, that is not to be restricted to small amplitude movements, must include that fact.

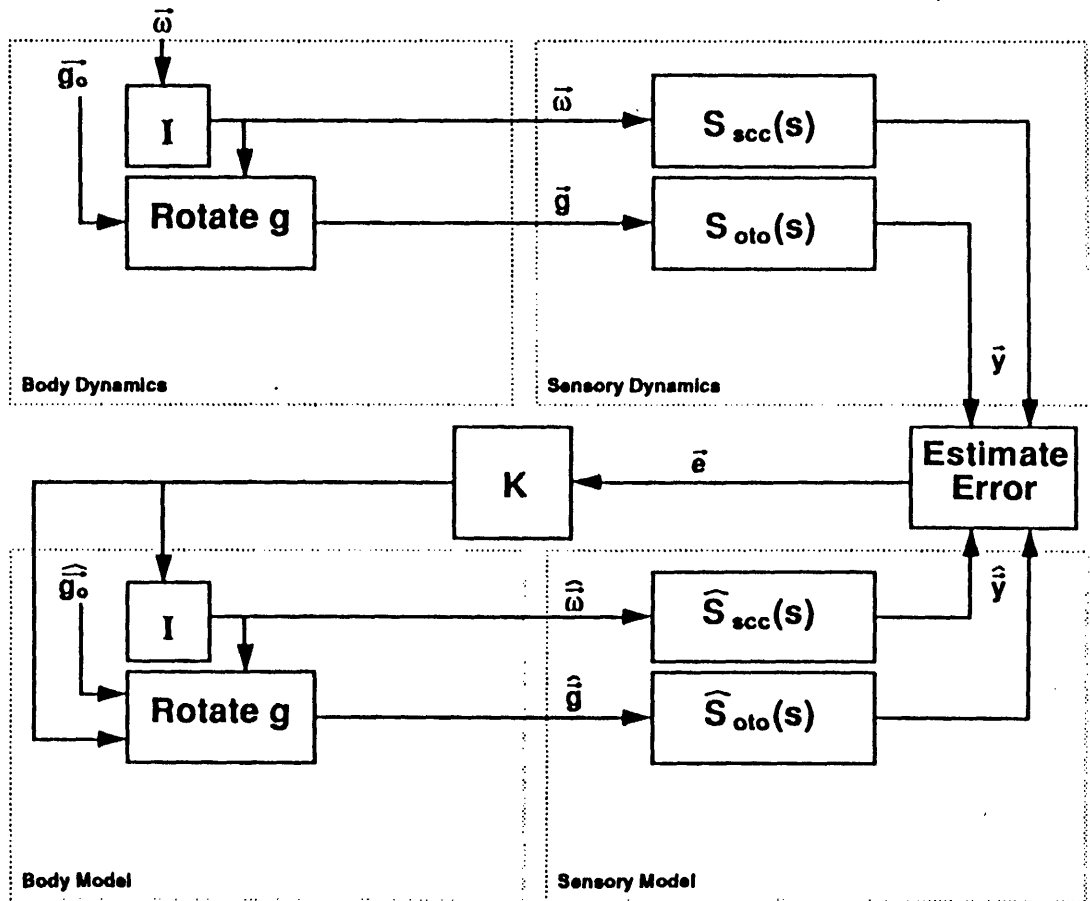
Dan Merfeld developed the model of Figure 4.3 to confirm his hypotheses, on the basis of centrifuge experiments.

The variables Scc and Soto represent the dynamics of the semicircular canals and otoliths respectively. The block "Rotate g" contains the calculation of the components of the gravitational vector in the head coordinates. Mathematically, knowing the angular velocity as a function of time, $\omega(t)$, allows us to calculate the transformation matrix B, between the earth and the head coordinate systems.

$$\omega = \begin{pmatrix} \omega_1 \\ \omega_2 \\ \omega_3 \end{pmatrix} \quad \Omega = \begin{bmatrix} 0 & -\omega_3 & \omega_2 \\ \omega_3 & 0 & -\omega_1 \\ \omega_2 & \omega_1 & 0 \end{bmatrix}$$

MERFELD'S MODEL

THREE DIMENSIONAL SENSORY CONFLICT MODEL



From Merfeld [16]

$$\dot{B} = \Omega B$$

However, since B is a (3X3) matrix, this last equation is a set of 9 simultaneous differential equations.

A nicer way of calculating B was developed by mathematicians in the spirit of finding an equivalent in three dimensions of what the complex numbers are in two dimensions. They defined the "quaternions" as expressions of the form:

$$q = q_0 + q_1 i + q_2 j + q_3 k$$

with

$$i^2 = j^2 = k^2 = -1$$

$$i.j = -j.i = k$$

$$j.k = -k.j = i$$

$$k.i = -i.k = j$$

Our goal here is not to explain the algebra of the quaternion field, which is done in all advanced algebra textbooks ([25] has a good chapter on it, albeit in French!). Let us just say that a rotation of angle θ about an axis u can be represented by a quaternion

$$q = \cos(\theta/2) + \sin(\theta/2)(u_1 i + u_2 j + u_3 k)$$

Note that the dimension of a quaternion is four, which is the dimension of a rotation (1 for the angle and three for the axes). The equivalent of our 9 simultaneous differential equations is then going to be reduced to four in quaternion space. It can be shown that B is the solution of the following system:

$$\dot{q} = \frac{1}{2} \begin{bmatrix} 0 & -\omega_1 & -\omega_2 & -\omega_3 \\ \omega_1 & 0 & \omega_3 & -\omega_2 \\ \omega_2 & -\omega_3 & 0 & \omega_1 \\ \omega_3 & \omega_2 & -\omega_1 & 0 \end{bmatrix} q \quad q = \begin{bmatrix} q_0 \\ q_1 \\ q_2 \\ q_3 \end{bmatrix}$$

$$B = \begin{bmatrix} q_0^2 + q_1^2 - q_2^2 - q_3^2 & 2(q_1 q_2 - q_0 q_3) & 2(q_1 q_3 + q_0 q_2) \\ 2(q_1 q_2 + q_0 q_3) & q_0^2 + q_2^2 - q_1^2 - q_3^2 & 2(q_3 q_2 - q_0 q_1) \\ 2(q_1 q_3 - q_0 q_2) & 2(q_2 q_3 + q_0 q_1) & q_0^2 + q_3^2 - q_1^2 - q_2^2 \end{bmatrix}$$

Another property of the quaternion vector, which turns out to be very useful in filtering problems, is that its norm is 1. In other words:

$$q_1^2 + q_2^2 + q_3^2 + q_4^2 = 1$$

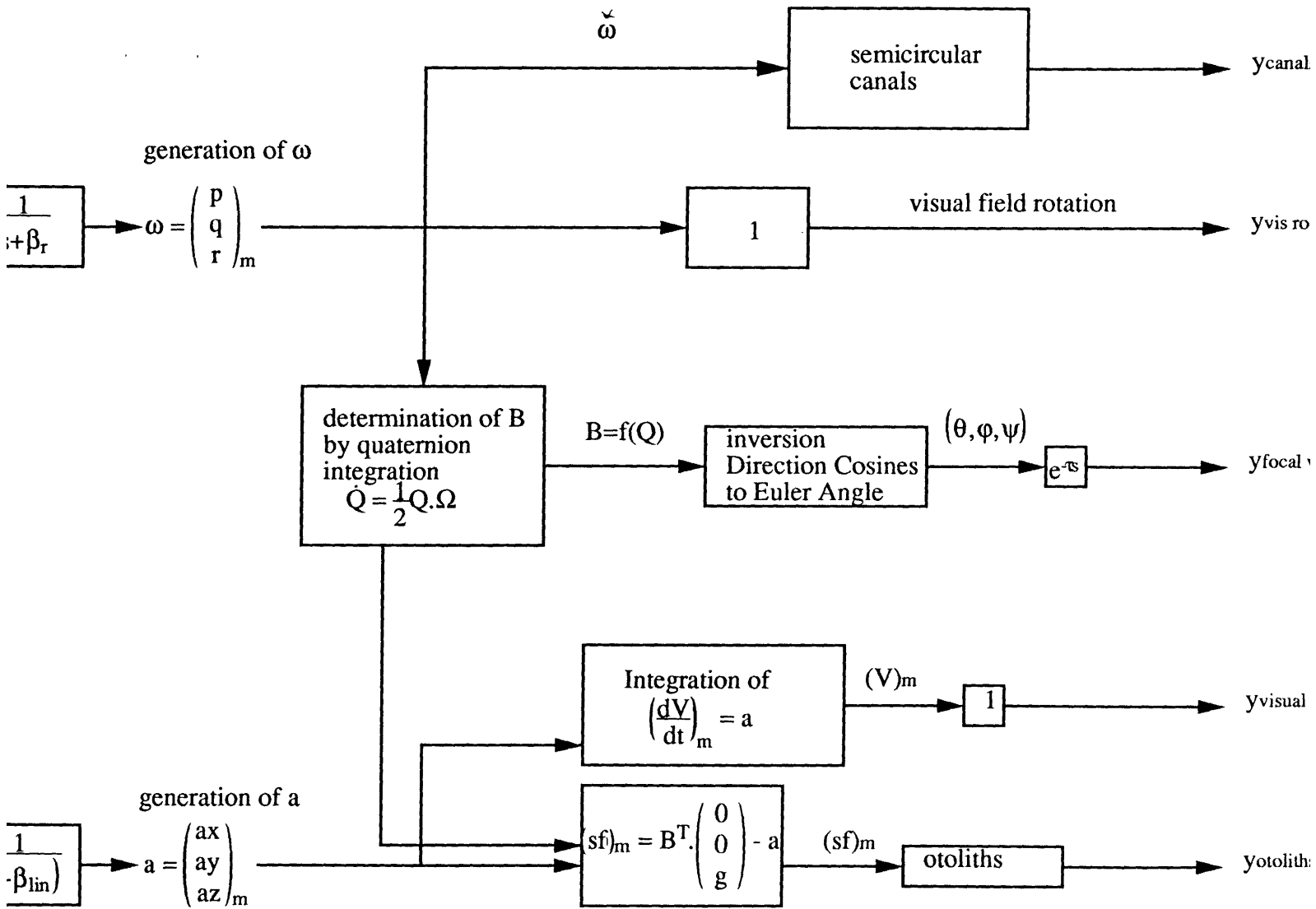
Those equations were implemented in Merfeld's internal model in the block "rotate g". But the gain used in [16] is not the solution of an optimization as in Borah et al. It is rather a matrix of chosen numbers that turn out to give adequate matching with the experiments. As the two approaches were very similar, we have tried in this thesis to link them via a new model that would incorporate a quaternion integration and an optimization of the gain under a minimum variance criterion. As the internal model is not going to be linear, the approach chosen is a suboptimal estimation technique in the form of the Extended Kalman Filter.

4.2 New Internal Model for the Central Nervous System

The main hypothesis in Borah's work is that the subject is expecting a certain frequency bandwidth in angular velocity and linear acceleration. We will assume the same in this work. Only we will consider here a first order shaping filter for the angular velocity instead of a second order as in Borah's model. The reason is that they needed a second order to create a differential equation for the angular acceleration that appeared as the input of the semicircular canals dynamics. Since we have chosen the angular velocity as an input (by adding an "s" to the numerator of the transfer function), there was no need for a second order filter which increases by three the dimension of the state vector.

The role of the vision in the orientation process is expressed in terms ofvection (circular and linear), or direct measurement of the angular and linear velocity. However, the pilot who is looking outside or at the instrument panel, is able to obtain a direct measurement of the orientation angles themselves. Expressed in terms of our model, the orientation angles, or Euler angles, are obtained via an algebra which is given in Appendix A.

NEW INTERNAL MODEL



This kind of measurement equations were implemented in Borah's model, and turned out to add little improvement (as the orientation angles were directly in the state vector, the implementation was rather easy). We decided not to consider those terms in this work.

4.2.1 State Vector Propagation

The block diagram of Figure 4.4 can be written in a state-space differential equation of the form:

$$\dot{x} = f(x) + \xi$$

x is a state vector of dimension 25, expressed in the head referential and partitioned as follows:

(x_1, x_2, x_3, x_4)	quaternion vector
(x_5, x_6, x_7)	angular velocity
(x_8, x_9, x_{10})	linear velocity
(x_{11}, x_{12}, x_{13})	linear acceleration
$(x_{14}, x_{15}, x_{16}, x_{17}, x_{18}, x_{19})$	semicircular canal afferent firing rates
$(x_{20}, x_{21}, x_{22}, x_{23}, x_{24}, x_{25})$	otolith afferent firing rates

Rewriting the quaternion integration in terms of the state vector gives:

$$\begin{aligned}\dot{x}_1 &= \frac{1}{2}(-x_5x_2 - x_6x_3 - x_7x_4) \\ \dot{x}_2 &= \frac{1}{2}(x_5x_1 + x_7x_3 - x_6x_4) \\ \dot{x}_3 &= \frac{1}{2}(x_6x_1 - x_7x_2 + x_5x_4) \\ \dot{x}_4 &= \frac{1}{2}(x_7x_1 + x_6x_2 - x_5x_3)\end{aligned}$$

If the subject expects a certain bandwidth of frequency in angular velocity β_r , this signal is represented in the internal model by the output of a first order shaping filter, or:

$$\dot{x}_5 = -\beta_{r1}x_5 + \xi_1$$

$$\dot{x}_6 = -\beta_{r2}x_6 + \xi_2$$

$$\dot{x}_7 = -\beta_{r3}x_7 + \xi_3$$

The values of the three frequency bandwidths need not be the same for the three axes. ξ is a white noise vector of zero mean, and covariance matrix Q1 which is supposed to be diagonal.

The linear velocity is the integration of the linear acceleration, which is also expected to be the output of a first order shaping filter, driven by a white noise ζ with a diagonal covariance matrix Q2.

$$\dot{x}_8 = x_{11}$$

$$\dot{x}_9 = x_{12}$$

$$\dot{x}_{10} = x_{13}$$

$$\dot{x}_{11} = -\beta_{11}x_{11} + \zeta_1$$

$$\dot{x}_{12} = -\beta_{12}x_{12} + \zeta_2$$

$$\dot{x}_{13} = -\beta_{13}x_{13} + \zeta_3$$

We have seen in Chapter 3 that the dynamics of the semicircular canal afferences could be described in term of a transfer function having the angular velocity as input. We gave acceptable values for the different time constants that are involved and we are going to suppose that those dynamics are the same for the three axes. Using the canonical correspondence between transfer function and state space representations, we end up getting:

$$\dot{x}_{14} = x_{15}$$

$$\dot{x}_{15} = -0.02075x_{14} - 0.1792x_{15} + x_5$$

$$\dot{x}_{16} = x_{17}$$

$$\dot{x}_{17} = -0.02075x_{16} - 0.1792x_{17} + x_6$$

$$\dot{x}_{18} = x_{19}$$

$$\dot{x}_{19} = -0.02075x_{18} - 0.1792x_{19} + x_7$$

Also, as seen in Chapter 3, the otoliths are considered as dynamic systems of second order, having the specific force as input. That specific force is the vectorial difference between the gravitation vector and the applied acceleration. Expressed in head coordinates, we get:

$$sf = B^T \begin{bmatrix} 0 \\ 0 \\ 9.81 \end{bmatrix} - a$$

The acceleration of the gravity is expressed in m/s. As B and a can both be expressed in terms of our state vector, we get:

$$sf_1 = 19.62(x_2x_4 - x_1x_3) - x_{11}$$

$$sf_2 = 19.62(x_4x_3 - x_1x_2) - x_{12}$$

$$sf_3 = 9.81(x_1^2 + x_4^2 - x_2^2 - x_3^2) - x_{13}$$

The equations for the otolith afferent rates being:

$$\dot{x}_{20} = x_{21}$$

$$\dot{x}_{21} = -100.1x_{20} - 10x_{21} + sf_1$$

$$\dot{x}_{22} = x_{23}$$

$$\dot{x}_{23} = -100.1x_{22} - 10x_{23} + sf_2$$

$$\dot{x}_{24} = x_{25}$$

$$\dot{x}_{25} = -100.1x_{24} - 10x_{25} + sf_3$$

4.2.2 Measurement Equations

The measurement equations are easily derived from the state space representation of the canals and otoliths transfer function, and from the fact that vection is supposed to provide a measure of the angular and linear velocity. We thus have:

$$\begin{aligned}y_1 &= -0.002075x_{14} - 0.1792x_{15} + x_5 \\y_2 &= -0.002075x_{16} - 0.1792x_{17} + x_6 && \text{canals afferent rates} \\y_3 &= -0.002075x_{18} - 0.1792x_{19} + x_7 \\y_4 &= x_5 \\y_5 &= x_6 && \text{angular vection} \\y_6 &= x_7 \\y_7 &= x_8 \\y_8 &= x_9 && \text{linear vection} \\y_9 &= x_{10} \\y_{10} &= x_{20} \\y_{11} &= x_{22} && \text{otoliths afferent rates} \\y_{12} &= x_{24}\end{aligned}$$

Finally, the fact that the norm of the quaternion vector is unity, can be implemented as a measurement equation in the filter.

$$y_{13} = x_1^2 + x_2^2 + x_3^2 + x_4^2$$

The measurement value corresponding to that equation being 1 all the time. This “trick” turns out to be essential in the filtering process. Actually, if we don’t use it, the norm of the quaternion can differ dramatically from 1, and then this vector becomes meaningless in terms of correspondence with the transformation matrix. Values of the quaternion vector and its norm are given in Appendix B.

Note finally that this last measurement equation is nonlinear.

4.3 Structure of the Central Nervous System

The problem is now stated in the form of the estimation of a random vector having a set of measurements and under the constraint of estimated dynamics. However, the problem of estimating a nonlinear process is recognized to be much more complicated than the linear case. The main reason is that the gaussian property of the stochastic process is not necessarily propagated throughout in nonlinear systems. Actually, in the linear case, gaussian assumptions on the initial conditions and the different noises allow us to calculate the conditional mean, - which is then equal to the minimum variance and the maximum likelihood estimates- as a linear operation on the measurement data, which is known as the Kalman Filter. In the nonlinear case, Bayesian estimation, or the optimization of the conditional probability density function, leads to estimates that are different from the conditional mean.

An approximate approach can, however, be taken in order to come up with an algorithm to calculate an estimate, suboptimal in a minimum variance sense (meaning that it would be optimal if all the simplifying assumptions were true). Considering, for instance, that the estimate is close to the real value of the state vector, we can write that:

$$f(x) = f(\hat{x}) + \left(\frac{\partial f}{\partial x} \right)_{x=\hat{x}} \cdot (x - \hat{x}) + o((x - \hat{x})^2)$$

with the residual term being very small and, hence, neglected. This first order linearization about the estimate allows the propagation of the covariance of the estimation error along the trajectory and leads to an algorithm known as the Extended Kalman Filter. This algorithm has been very popular in the world of engineering since the mid-sixties (among others it helped man to reach the moon, having been implemented in the onboard computer of the Apollo spacecraft [19]).

A good derivation of this filter, and of the general estimation problem, can be found in Gelb's book [20] on optimal estimation. Given initial conditions on the estimation error, mean and covariance, and given the statistics of the noise involved, the Extended Kalman Filter for a continuous process with discrete measurements can be described as follows:

Between two measurements, the propagation of the estimate occurs according to the equation:

$$\begin{aligned}\hat{\mathbf{x}} &= \mathbf{f}(\hat{\mathbf{x}}) \\ \dot{\mathbf{P}} &= \mathbf{F}(\hat{\mathbf{x}}) \cdot \mathbf{P} + \mathbf{P} \cdot \mathbf{F}(\hat{\mathbf{x}})^T + \mathbf{Q}\end{aligned}$$

The estimate is propagated with its covariance matrix until the measurement time, ending up with the values:

$$\hat{\mathbf{x}}^- \text{ and } \mathbf{P}^-$$

At the measurement time, update of the estimate occurs according to:

$$\begin{aligned}\hat{\mathbf{x}}_+ &= \hat{\mathbf{x}}^- + \mathbf{K}(z_k - h(\hat{\mathbf{x}}^-)) \\ \mathbf{P}_+ &= (\mathbf{I} - \mathbf{K} \cdot \mathbf{H}(\hat{\mathbf{x}}^-)) \cdot \mathbf{P}^- \\ \mathbf{K} &= \mathbf{P}^- \cdot \mathbf{H}(\hat{\mathbf{x}}^-) \cdot (\mathbf{H}(\hat{\mathbf{x}}^-) \cdot \mathbf{P}^- \cdot \mathbf{H}(\hat{\mathbf{x}}^-)^T + \mathbf{R})^{-1},\end{aligned}$$

where \mathbf{P} is the covariance of the estimation error, \mathbf{Q} the covariance of the driving noise, \mathbf{R} the covariance of the measurement noise, and:

$$\mathbf{F}(\hat{\mathbf{x}}) = \left(\frac{\partial \mathbf{f}}{\partial \mathbf{x}} \right)_{\mathbf{x}=\hat{\mathbf{x}}}$$

$$\mathbf{H}(\hat{\mathbf{x}}) = \left(\frac{\partial h}{\partial \mathbf{x}} \right)_{\mathbf{x}=\hat{\mathbf{x}}}$$

There is of course a lot to say about this algorithm, but we will restrict ourselves to a few comments. First, there are no rules for the convergence of the filter. As the computation of the gain involves the estimate itself, which is a random vector, the gain is also stochastic. In the linear case, the gain could be calculated "off-line" from a Riccati differential equation. Here the gain is the solution of a stochastic differential equation for which very few convergence results are available. The performance of the filter has then to be tested by Monte Carlo simulations. Second, the algorithm turns out to be very sensitive to initial conditions due to the first order approximation. If the initial estimate is too far from the real solution, the filter is going to diverge in most of the cases. Third, the computation of the gain involve the inversion of a matrix which can lead to numerical problems, if the matrix $(HPH'+R)$ is too small or close to singular.

If we now suppose that the Central Nervous System is "trying" to optimize a kind of minimum variance criterion, given measurements and estimated dynamics, we can say that the internal representation of the state vector will be close to the solution of the Extended Kalman Filter applied to our model. In other words, our basic assumption is to say that the Central Nervous System is an Extended Kalman Filter.

As a conclusion to this chapter in which we have presented a model for the Central Nervous System we can make a few comments. The basic problem of finding an orientation or a position in space using instruments that are related to the moving body is closely related to the inertial navigation of vehicles using "strap-down" systems¹. In other words, the vestibular

¹ Inertial navigation uses gyroscopes and accelerometers to calculate the position and velocity in space of a moving vehicle. A classical way of navigating with inertial instruments, is to use the gyroscopes to stabilize, in an inertial space, a platform on which the accelerometers are set up. The gravity vector is added to the measurement of the accelerometers, the ensemble being integrated two times to find the position. A "strap-down" system is an inertial navigator where the instruments are linked to the vehicle and, therefore, give measurements in the moving coordinates. A quaternion integration is then necessary to keep track of the position of the gravity vector in the navigation loop.

system can be understood as an inertial platform, providing measurements of the angular velocity and the specific force applied to the CNS. It is then not surprising to include a quaternion integration in the system, knowing that it is part of the mechanization of the “strap-down” inertial navigation system as well. Also, representing an unknown acceleration, in a filter which involves measurements of velocities, by the output of a shaping filter driven by a white noise process is frequently used in estimation problems. An example that we have in mind is the estimation of the trajectory of a ballistic missile, using angular measurements of the position and Doppler measurements of the velocity. However, let us keep in mind that human mechanisms are certainly much more complex than all models which try to represent them.

Chapter 5

Implementation Considerations and Simulation Results

5.1 Time History Generation

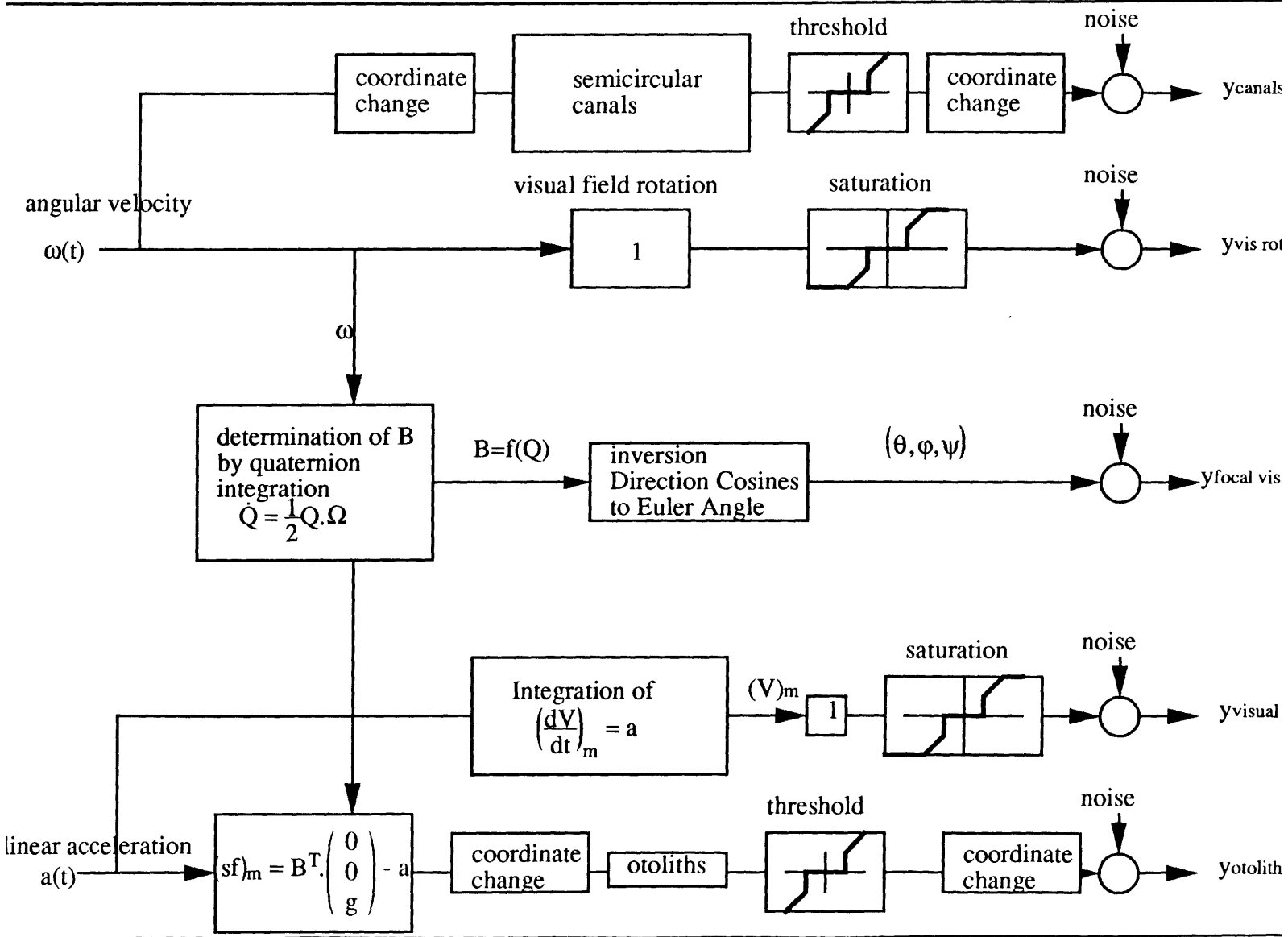
In order to study the mechanism of the Central Nervous System, modeled as an Extended Kalman Filter, we need to generate the set of measurements corresponding to the outputs of the human sensors in a particular situation. Such a situation can be characterized by the definition of two functions of time: the angular velocity and the linear acceleration.

Actually, the angular velocity provides the input to the semicircular canal dynamics ending up with the canals afferences. It also activates the quaternion integration which keeps track of the position of the head referential. Also, combined algebraically with the gravitation vector, the linear acceleration provides the specific force which becomes the input to the otolith dynamics.

In a more general closed-loop model, like Oman's model as in Figure 1.1, the angular velocities and linear acceleration would be the output of the dynamic equations of the vehicle, given the pilot's control. Here, we consider an open-loop model, in which the subject has no control of the movement of the vehicle. The angular velocities and linear accelerations are then precalculated and used as input to a "Time History Model".

The model of Figure 5.1 is close to the internal model of Figure 4.4. Actually, the "Internal Model" stands for the internal representation of that "Time History Model". However, a few differences need to be pointed out. First, in trying to represent reality as closely as possible, the "Time History Model" includes the nonlinearities that we've described earlier as well as thresholds for the vestibular cues, and thresholds and saturations for the visual cues. Second, the nonlinearities operate on the canals and otoliths sensitive axes.

TIME HISTORY GENERATION



In other words, we need to transform the entering signals, which are given in “head coordinates”, into the canal and otolith coordinates before applying the transfer functions and the nonlinearities.

5.2 Computer Implementation

The model was implemented on a Macintosh II, using the software Mac II-MatLab, ©The MathWork, Inc. The advantage of such a language is of course the ease of use for matrix manipulations. The main problem, however, is computation time. A 30 second simulation on MatLab takes 4 hours! But for a first iteration in the model design, where the model outputs are tested on simple and understandable simulations, this software support turned out to be adequate.

The basic structure of the computer simulation, for our model of spatial orientation is as follows:

- Initialization of the parameters of the “Time History Generation” (thresholds, saturation and so on..)
- Generation of the angular velocities and linear accelerations as functions of time.
- Integration of the differential equation providing the set of measurements.
- Initialization of the state estimate and covariance error, along with the initialization of the internal model parameters (bandwidth of expected signal, covariance of the measurement noise).
- Integration of the Extended Kalman Filter.

5.2.1 Integration of the “Time History Generation”.

The mathematical model corresponding to the block diagram of Figure 5.1 is easily derived from the Internal Model developed in Chapter 4, with the addition of matrix transformation and nonlinear operations (actually, as we considered that the thresholds and saturations were calculated in the canal and otolith coordinates, the state vector needs to be

calculated in these reference frames before being transformed into “head coordinates”). We thus get a function of the form:

$$\dot{x}=f(x)+u(t)$$

where x is a state vector of the same size as the internal state vector and u is an input function containing the angular velocities and the linear accelerations. The numerical integration of such a nonlinear differential equation is done by a Runge-Kutta algorithm of the third order (the equations are given in Appendix C).

It can be proven that the numerical integration will converge if the integration step is chosen to be of the order of the shortest time constant involved in the system. This is one of the limitations for using the otolith dynamics suggested by Grant and Best [21]. As the model is not simple, using a time step of 0.0002s would make simulation last for ever, at least on MatLab. This is the main reason for which we have chosen a 0.01 second time constant for the otolith dynamics.

The afferent firing rates are then calculated at each time from the value x_k , and are stored in the columns of a large vector. The codes corresponding to those operations are given in Appendix C under the names:

- angvel** Angular Velocity as a function of time.
- linacc** Linear acceleration as a function of time.
- thmodel** Time History Model.
- RK3** Integration using a Runge-Kutta third order.
- AFR** Calculation of the afferent firing rates.

5.2.2 Extended Kalman Filter

We have chosen to implement a continuous-time filter with discrete measurements as developed in Chapter 4. The frequency of the measurement update has been set to 25 Hz, which is approximately the frequency of the visual information. The integration algorithm for the propagation equation is also a Runge-Kutta of the third order, with a 0.01s time step.

Assuming that the experiment is started at rest, the subject has very good initial knowledge of its spatial orientation. The quaternion vector then starts with the value (1,0,0,0), meaning that the head referential is initially aligned with the earth referential. Being only submitted to the gravitation before the start of the simulation, all of the states but one are assumed to be zero. Actually, only the state corresponding to the vertical axis in the otolith model is in steady state value. As the otolith dynamics is modeled by,

$$\ddot{x}+100.1\dot{x}+10x=sf$$

the steady state value corresponding to a constant specific force of 9.81 m/s² is $x_{ss}=0.981$.

The initialization of the covariance of the estimation error and the different noises reflects the skill of the subject in an experimental case. Actually, a well trained pilot will be more confident in his internal measures of spatial orientation than a novice. We can, therefore, take into account a certain expertise of the pilot by diminishing the values of the initial covariances.

We integrated the covariance equation using the same algorithm as before. We preferred, however, to use an equivalent form of the covariance update, called Joseph's Form, which has the advantage of keeping the positive definite form of the covariance matrix.

$$K=P \cdot H^T \cdot (H \cdot P \cdot H^T + R)^{-1}$$

$$P+=(I-K \cdot H) \cdot P \cdot (I-K \cdot H)^T + K \cdot R \cdot K^T$$

Actually, numerical errors due to the matrix inversion in the calculation of K can lead to the appearance of negative eigenvalues in P, which is, of course, not reasonable for a covariance matrix.

The measurement noise is added at each step to the measure coming from the “Time History Model” data, using signal-noise ratio, as in Borah et al [10]; Those ratios are parameters of the filter.

The corresponding codes are given in Appendix C as:

- model** Equation of the model propagation
- grad** Calculation of the gradient matrix
- filtering** Global simulation involving everything

5.3 Simulation Results, Comparison with Previous Studies

As a way of testing our model, we first simulate the cases that are used in Borah et al. Their basic simulations were a rotation stimulus about the yaw axis, and a forward acceleration along the x-axis.

5.3.1 Yaw Motion

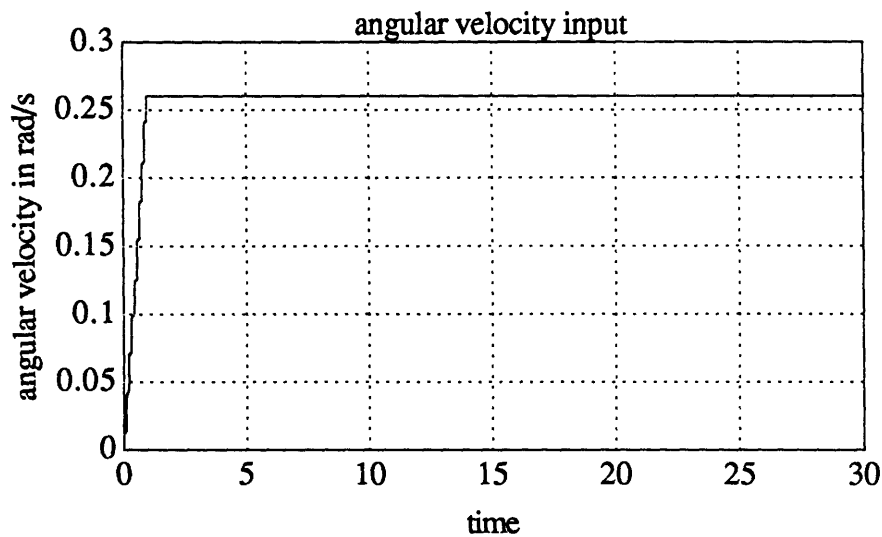


Figure 5.1

The input stimulus is the angular velocity about the yaw axis (z-axis) of Figure 5.1. The pitch and roll angular velocity and the linear accelerations are set to zero all the time. This

situation is comparable to a rotating chair experiment. We have chosen a simulation time of 30 seconds.

A plot of the semicircular canals afference is given in Figure 5.2

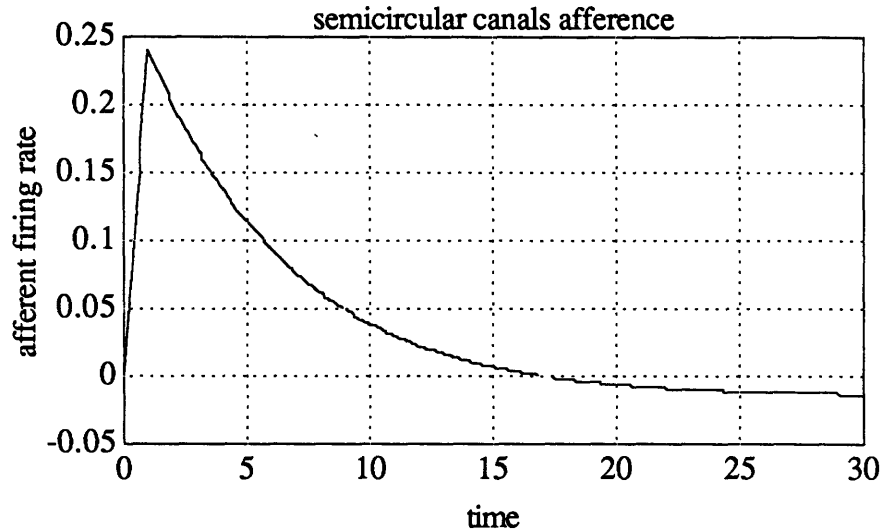


Figure 5.2

5.3.1.1 Rotation in the Light

The measurement set used for the filter includes the semicircular canals afference and the circular vection. The estimated value for the angular velocity is plotted in Figure 5.3. The estimation is almost perfect. This result was expected, since the filter has excellent knowledge of the angular velocity from the visual information. The quaternion vector turns out to be well integrated in the filter, providing the right angular orientation. This example was mainly used to set up the numerical parameters of the discrete-time integration.

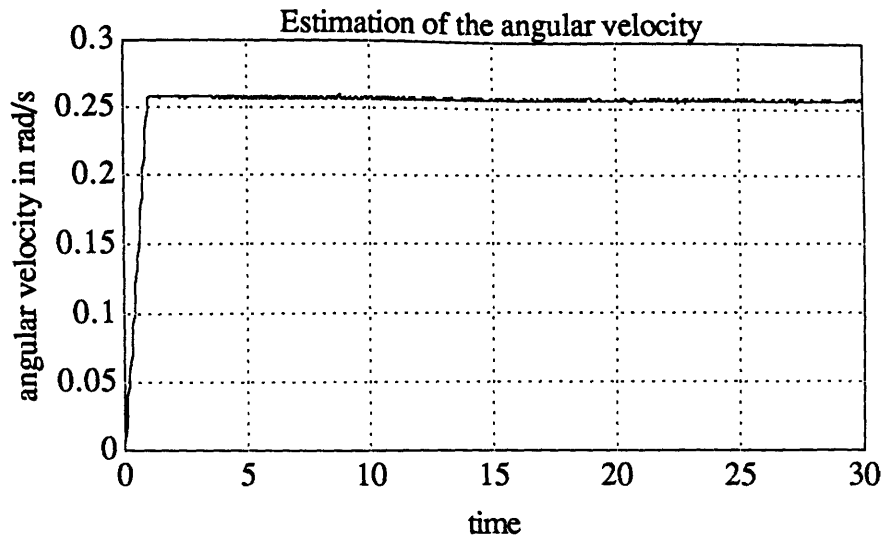


Figure 5.3

5.3.1.2 Rotation in the Dark

The rotation in the dark is simulated by taking out the visual measurement on the measurement vector. The CNS relies then only on the vestibular system.

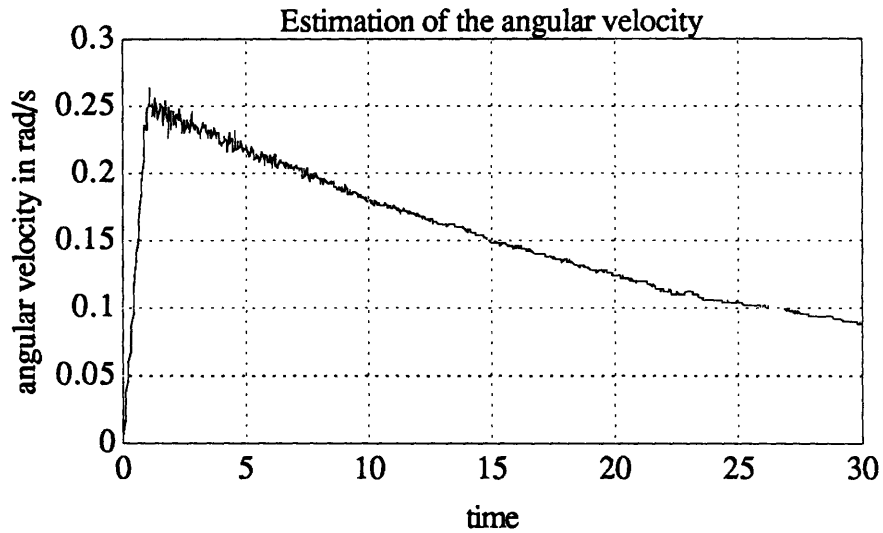


Figure 5.4

Figure 5.4 shows the well documented adaption to continuous rotation.

5.3.1.3 Circular Vection

By setting the vestibular afferent firing rate to zero, we can simulate the effect of circular vection.

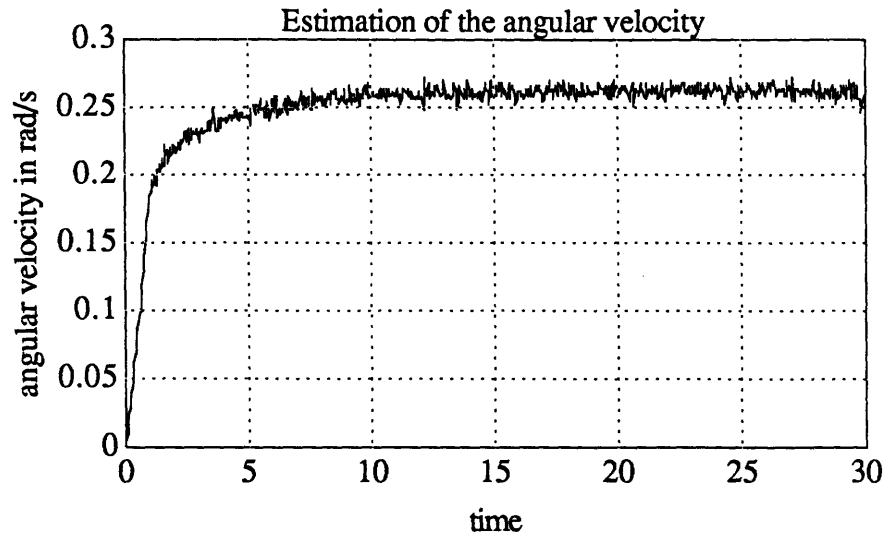


Figure 5.5

We can see the gradual acceptance of the angular velocity that has been proved experimentally. Borah et al [10] comment on that result that experimental records of visually induced movement were showing delays, whereas here, the onset on angular velocity sensation is shown to begin immediately after the onset of visual field motion. The fact that our model doesn't include physiological reaction to sensory conflict is certainly one of the reasons, along with the fact that the time-varying filter is much faster than the steady state filter. Borah et al "fixed" this manually by including a kind of switchable gain on the visual channel. We preferred not to do this manipulation, and refer the reader to our comments about possible improvements in the conclusion of this thesis.

The estimate of the quaternion vector turned out to give results that were coherent with the estimated angular velocity.

5.3.2 Forward Acceleration

Borah et al considered the case of a linear acceleration of 0.2g, reached after one second, and lasting throughout the experiment. In order to compare our model with theirs, we have used the same values.

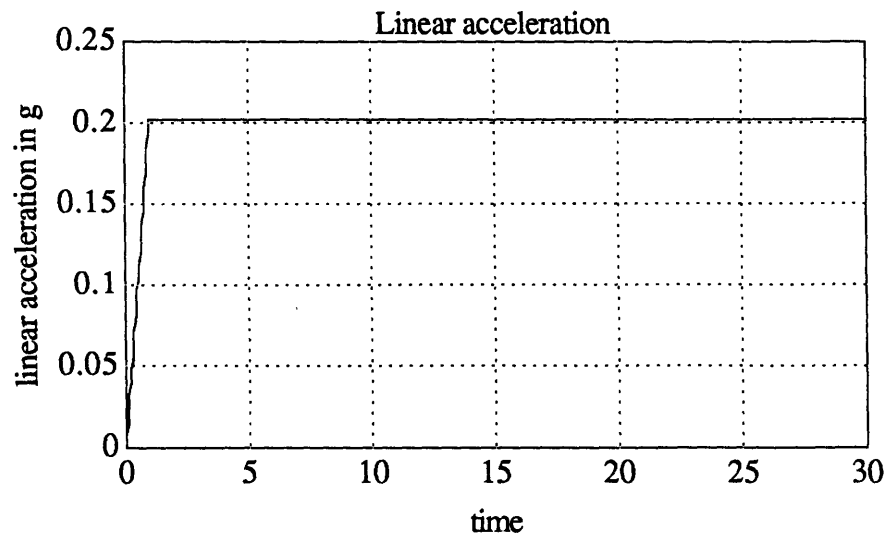


Figure 5.6

5.3.2.1 Acceleration in the Dark

When no visual cues are present, the estimated acceleration is progressively replaced by a pitch-up sensation as shown in Figures 5.7 and 5.8.

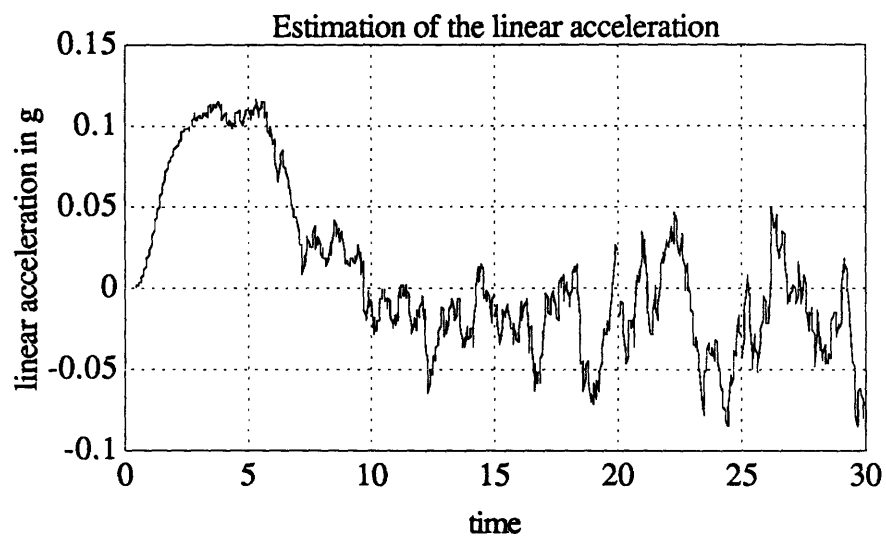


Figure 5.7

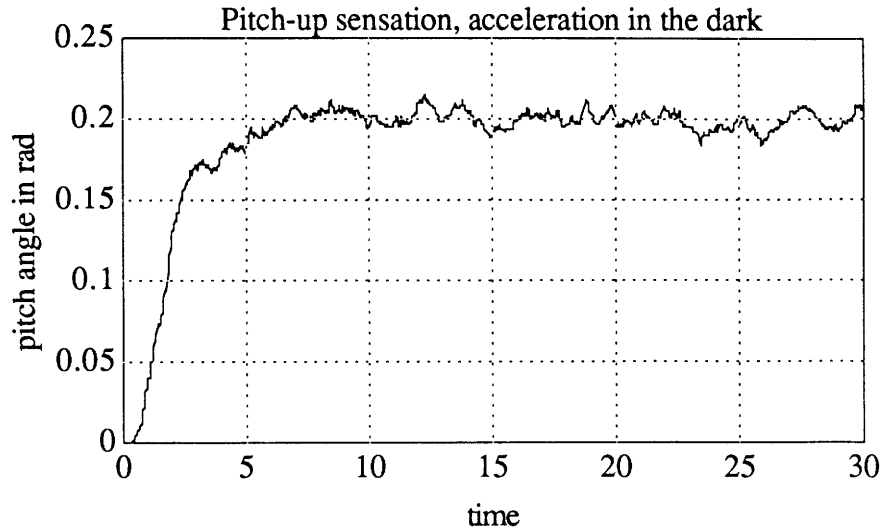


Figure 5.8

The estimated values are plotted as they come out from the filter, without any numerical filtering techniques. However, we can see that they are very noisy. Actually, this kind of estimation turns out to be very sensitive to numerical errors, especially in the quaternion integration part. As the noise added looked like white noise, and as the interesting signal has a very low frequency spectrum, a way of getting rid of it is to pass the result through a low-pass filter.

Due to the fact that the pitch angle sensation involved is very small, sufficiently small to validate a first order approximation, the model prediction is very similar to Borah's.

The fact that, in steady state, the CNS tends to interpret a linear acceleration by a pitch sensation, and that perceived specific force seems to be aligned with gravity has been confirmed in centrifuge experiments by Wolfe and Kramer [22].

5.3.2.2 Acceleration in the Light

We have seen previously that linearvection would provide information on the linear velocity up to a saturation value.

The filter interprets that hypothesis by considering that the linear acceleration is equal to zero when the speed has reached the saturation value, ending up with a pitch sensation.

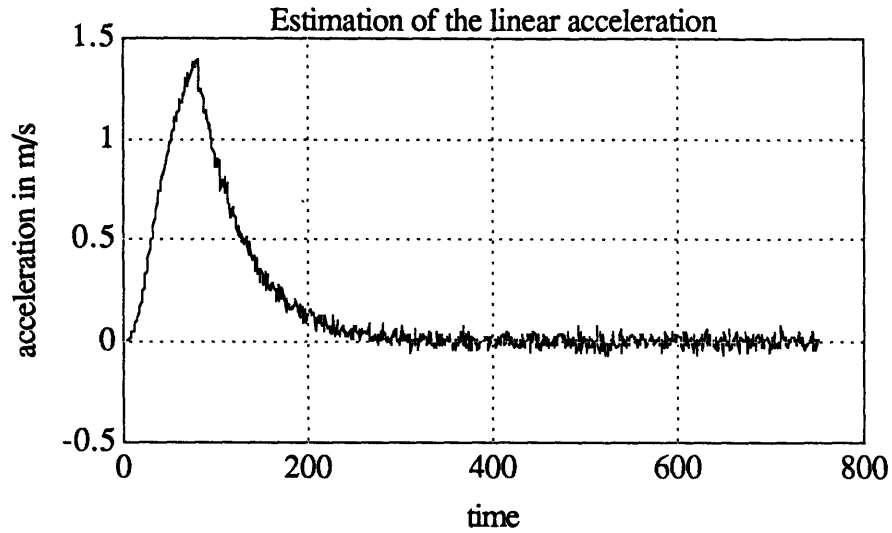


Figure 5.9

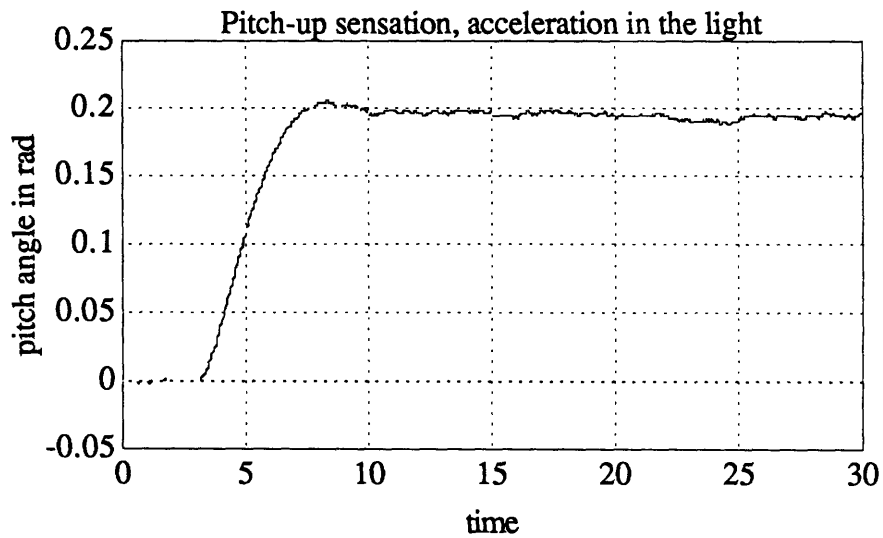


Figure 5.10

The plot of the estimation of the linear acceleration was passed through a low pass filter. We give in Figure 5.11 the estimated linear velocity. It is clear on the plot that the hypothesis of a brute saturation without changing parameters in the filter is a bit unrealistic.

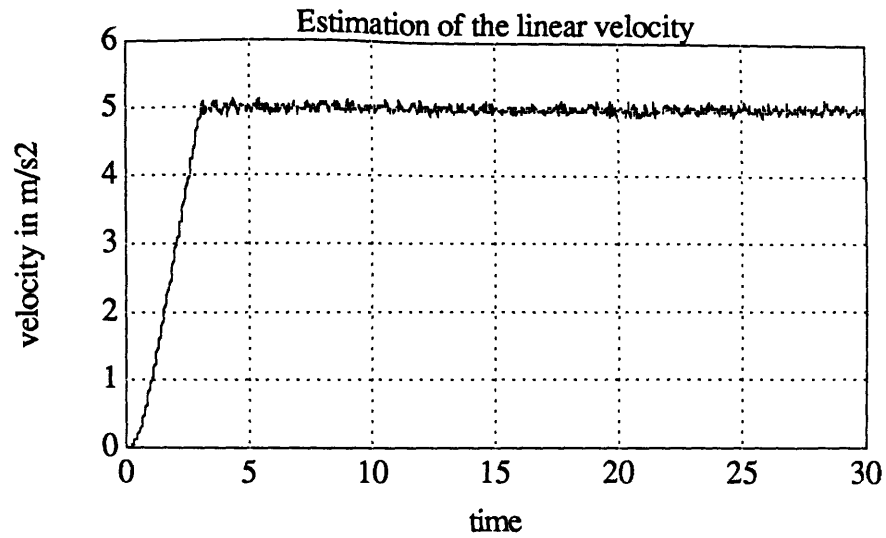


Figure 5.11

If, on the other hand, we consider that there are no saturation limits on the measurement of the linear velocity, the estimation of the linear acceleration turns out to be accurate, leading to no pitch sensation.

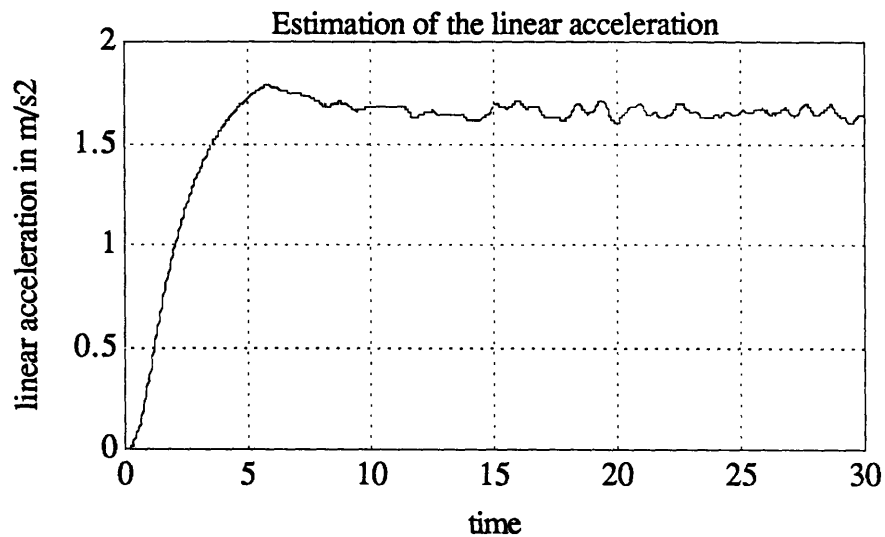


Figure 5.12

5.3.2.3 Linear Vection

Borah et al are considering the experimental case of Chu [23], where linear vection was experienced in front of a 15 cm/s moving field.

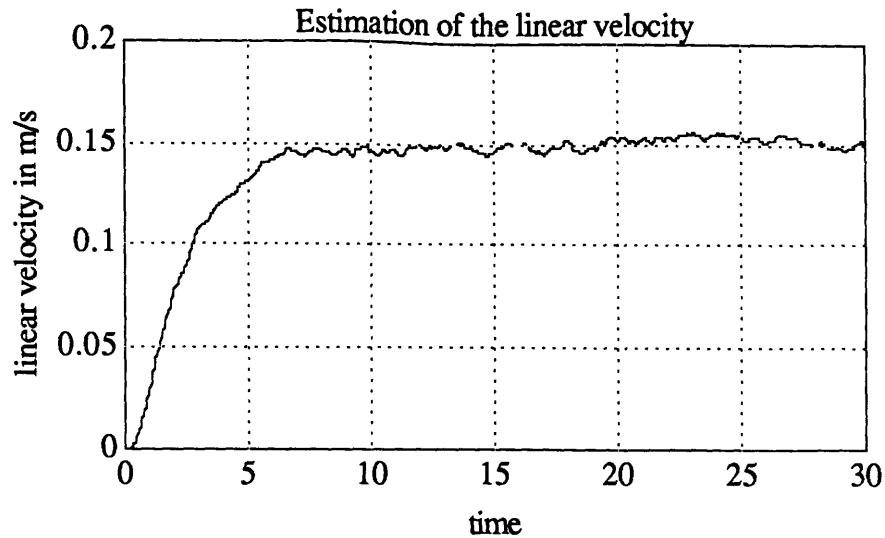


Figure 5.13

The model prediction agrees with the experiment, showing a gradual acceptance of visual field velocity. Once again, the model output is not showing the delays that are evident in experiments. We will discuss that point in our conclusion.

5.3.3 Tilting Motion

In the following figures, we present the model prediction to a rotation about the horizontal axis, or pitch axis, of an angle of 0.2 radians reached in 3 seconds. Figure 5.14 corresponds to a stimulus in the light, Figure 5.15 to the same in the dark, showing the estimated pitch angle, angular velocity and linear acceleration.

We note that, in both cases, the pitch angle and the angular velocity are well estimated. The illusion of linear acceleration is inexistent when visual cues are present, and very small in the “in the dark” case. This issue was unclear in Borah et al, who found a significant linear acceleration and quite bad estimation of the pitch angle. This is explained by the fact that a time varying Kalman Filter is much faster than the steady state filter, and also by the fact that the quaternion integration provides a more accurate estimate of the orientation angles.

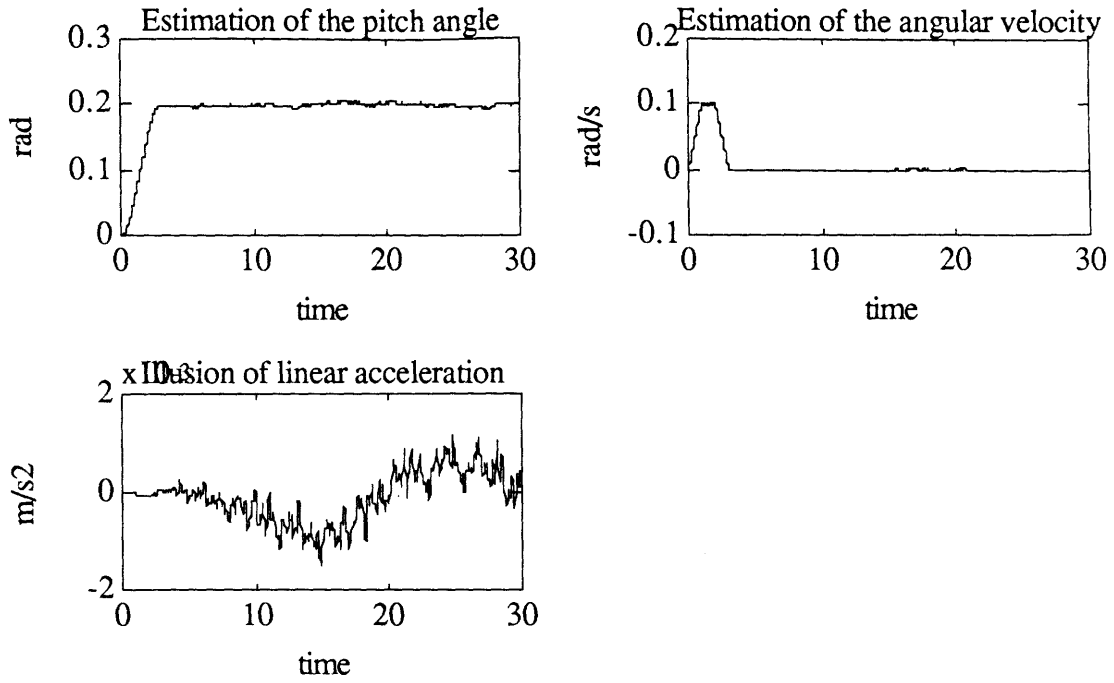


Figure 5.14, Pitch in the light

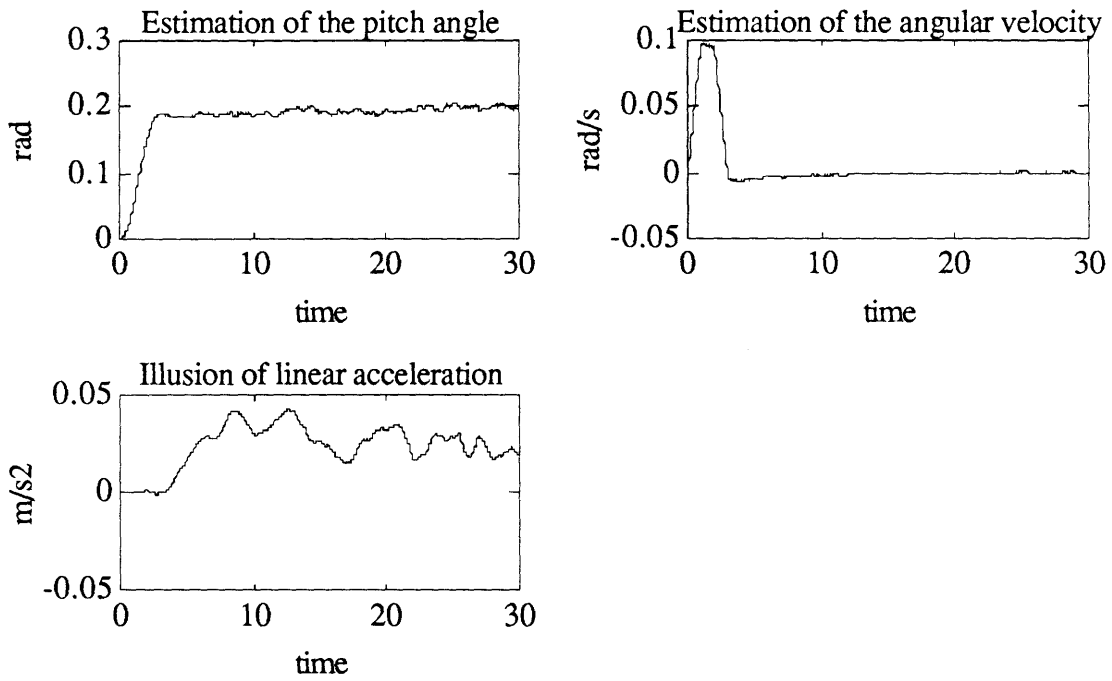


Figure 5.15, Pitch in the dark

5.4 Sensitivity to Filter Parameters

We have seen that the estimation algorithm, was parametrized by the "expected" frequency bandwidths of the internal model, and the measurement and driving noises. It is, therefore, interesting to study the sensitivity of the filter to those parameters.

5.4.1 Frequency Bandwidth in Angular Velocity

Figure 5.16 shows the results of the estimation of the angular velocity, in the experimental case of paragraph 5.1, and without visual cues ("in the dark"), for different values of the parameter br .

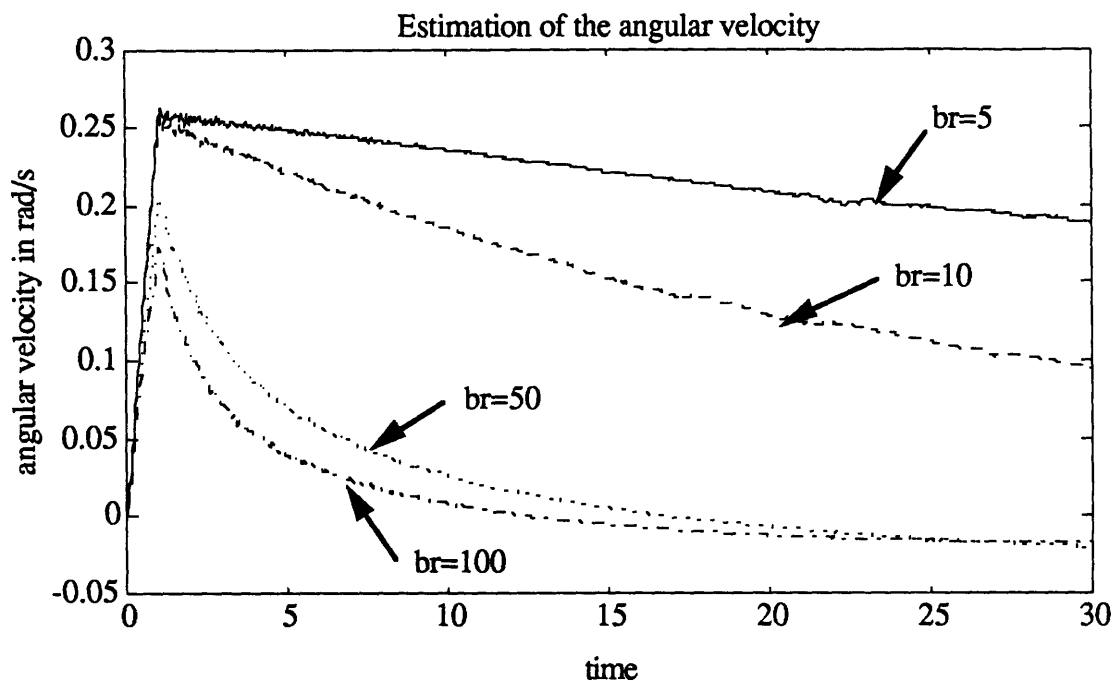


Figure 5.16

We can see that large expected frequency bandwidths lead to bad estimation of the angular velocity. Actually, the input is almost a "step" in angular velocity (having $1/s$ for Laplace transform), and if the internal model has the right description of the input signal, it can be

shown that the system is observable with the vestibular measurement. In other words, a small b_r gets the system closer to observability, and the estimation more accurate.

This parameter can be understood as a "skill" value, in the sense that someone who is used to rotating chair, might use, in his internal model, a smaller value of b_r than someone who is at his first try.

5.4.2 Frequency Bandwidth in Linear Acceleration

Figure 5.17 presents the estimation of the linear acceleration in the dark, with respect to different values of the "expected frequency bandwidth". Once again, as the input is almost a step in acceleration, the smaller the parameter the better the estimation. However, we note that in every case, the estimate goes to zero due to the associated pitch sensation.

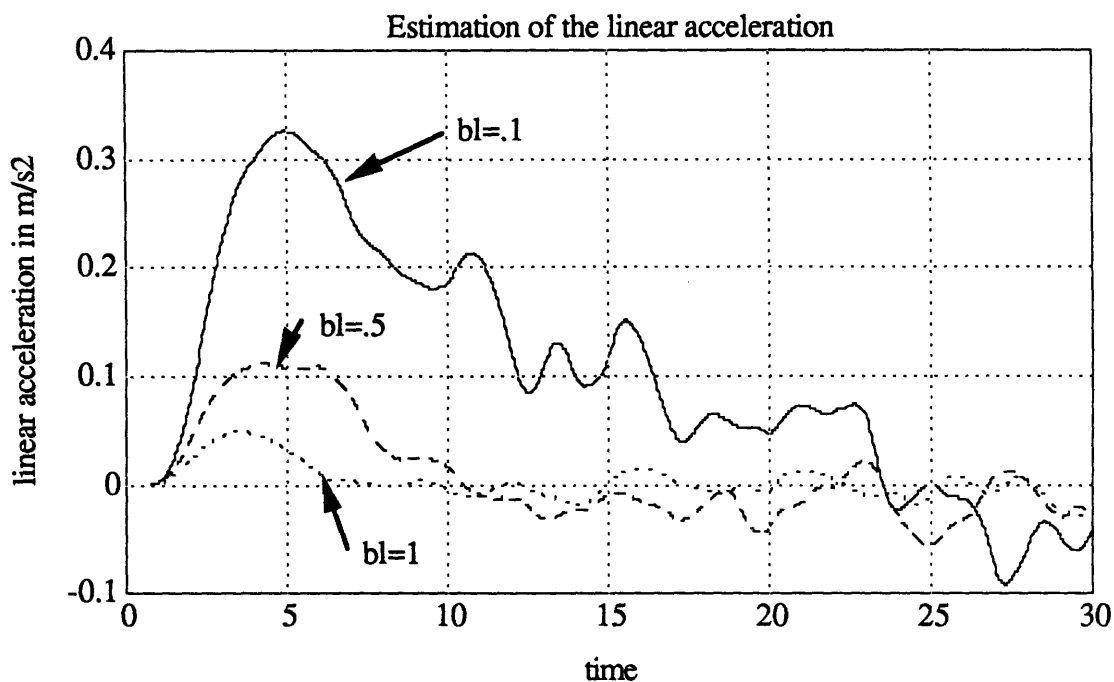


Figure 5.17

5.4.3 Driving Noise

The driving noise is the white noise that drives the internal representation of the angular velocity and linear acceleration. We have seen that those models were first order transfer

functions driven by white noise. In the filtering process, the driving noise is represented in terms of its covariance which affects the computation of the suboptimal gain. Figures 5.18 and 5.19 present the results of simulations in the dark for varying driving noise covariances on the linear acceleration case.

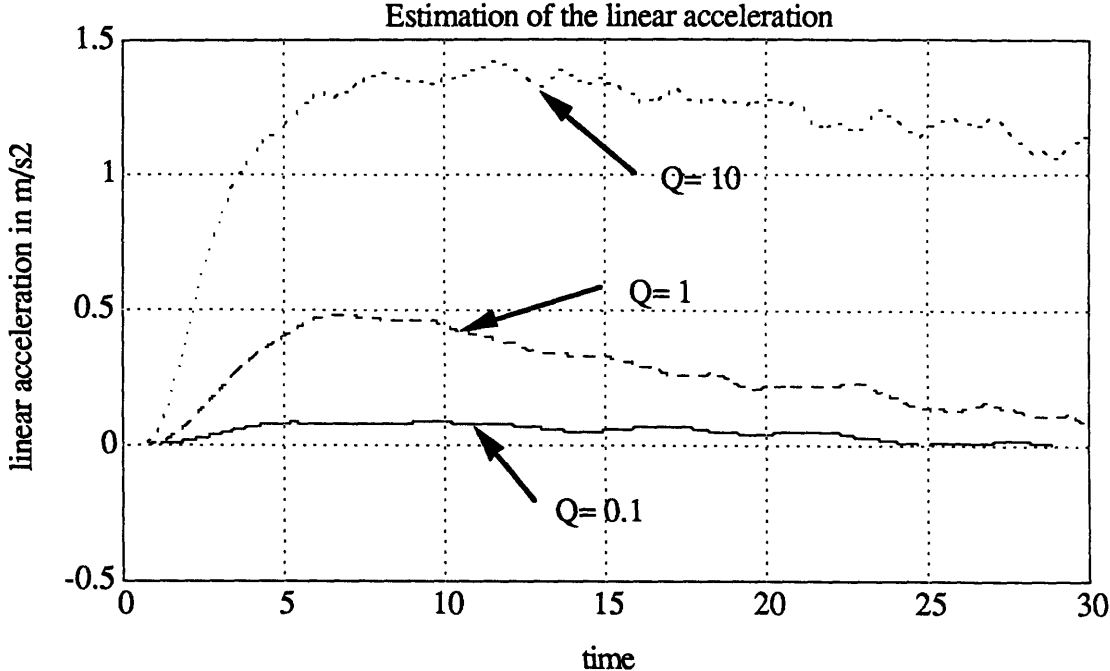


Figure 5.18

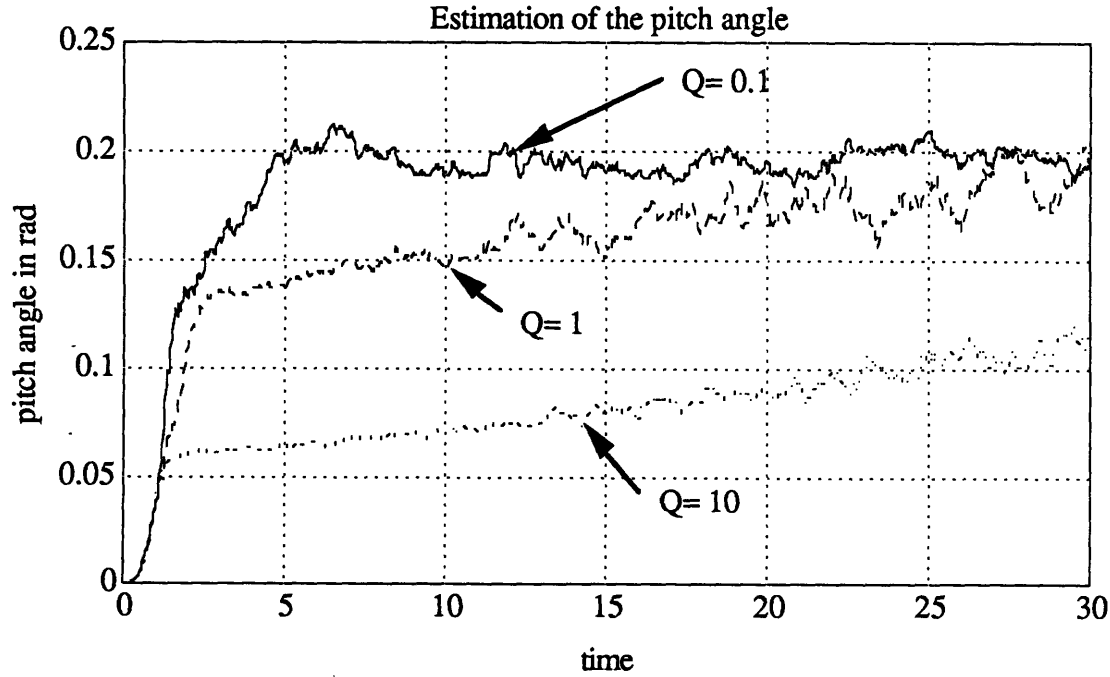


Figure 5.19

We can see that the covariance of the driving noise can dramatically affect the estimate of the linear acceleration and the pitch angle illusion.

Figure 5.20 shows the effect of the driving noise on the angular velocity channel.

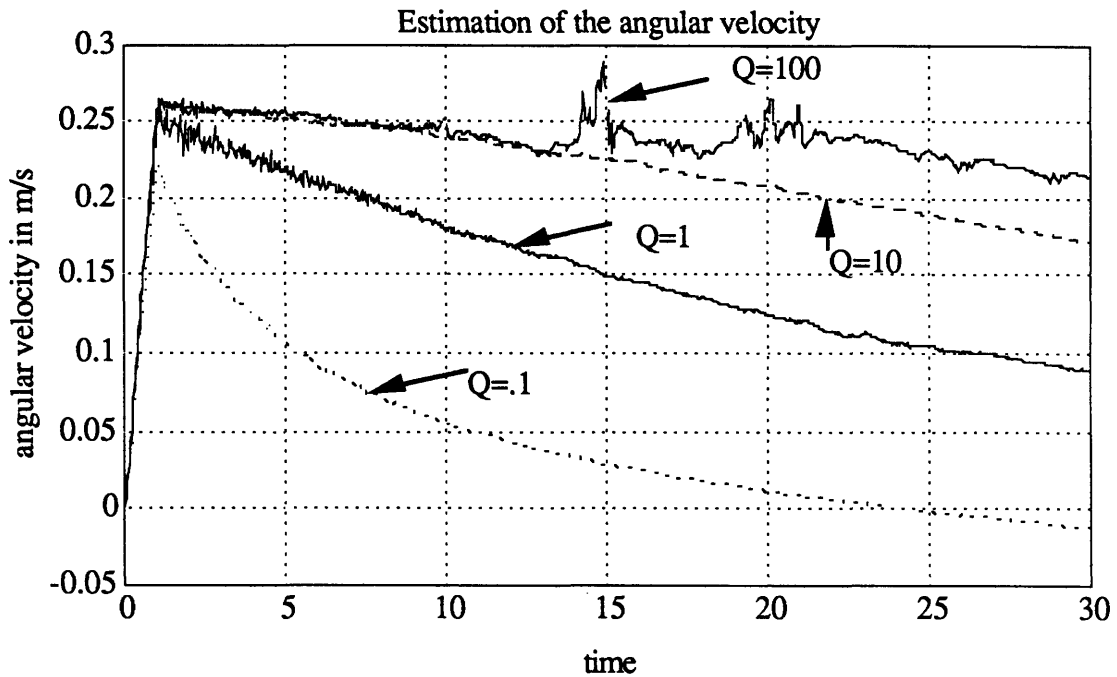


Figure 5.20

As in the preceding section, the estimation of the angular velocity can be tuned up by adjusting the covariance of the driving noise. However, we can see that numerical problems appear in the filter with large driving noises.

Intuitively, we try to fit a step function with a first order exponential. A small calculus on that reduced problem, can show that the dynamics of the estimator is basically inversely proportional to the driving noise. In other words, higher driving noises lead to slower dynamics and then better estimators.

5.4.4 Measurement Noise

As in Borah et al [10] we quantified the measurement noises by a signal-noise ratio. What we called R is the covariance of the measurement noise as referred to the cited reference. Figure 5.21 shows the predictions of our model for different measurement noises, in a “rotation in the dark” case.

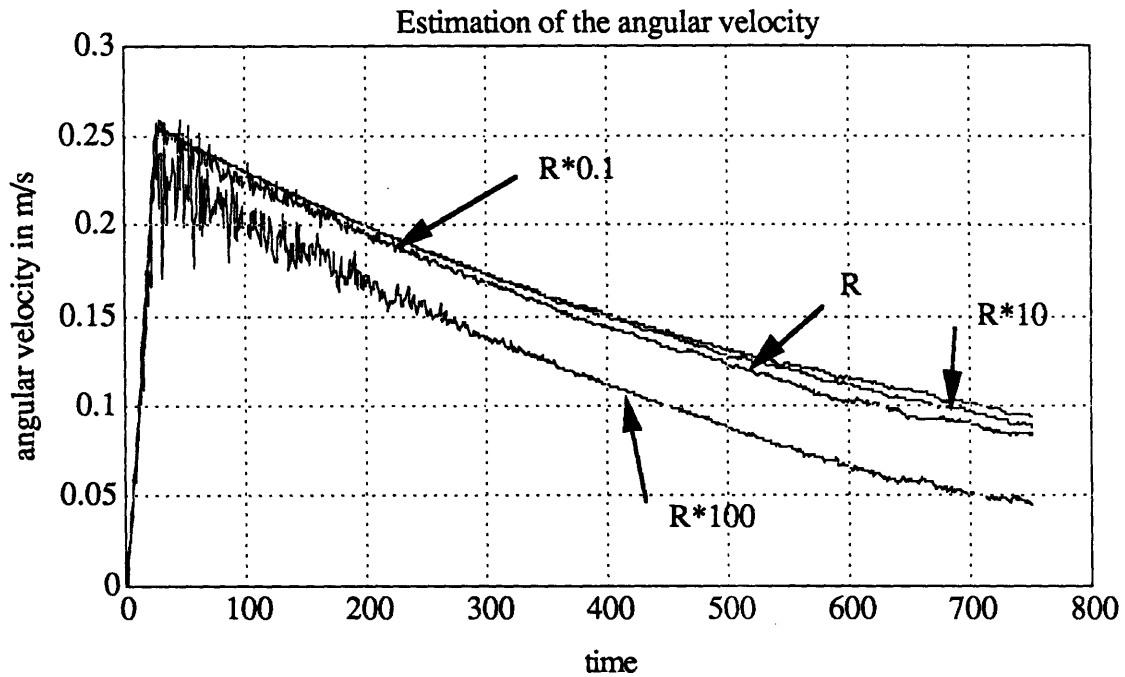


Figure 5.21

The filtering process turns out to be quite robust to measurement noise, the shape of the estimation of the angular velocity remaining the same throughout the simulations.

5.5 Centrifuge Experiment

Most of the experiments on which a spatial orientation model can be tested concern centrifuges. In order to generate the angular velocities and linear acceleration experienced in a centrifuge, we are going to consider a “simplified” model in which the specific force is always aligned with the vertical axis of the subject. We also suppose that the center of mass of the cabin is located at the junction with the rotating axis.

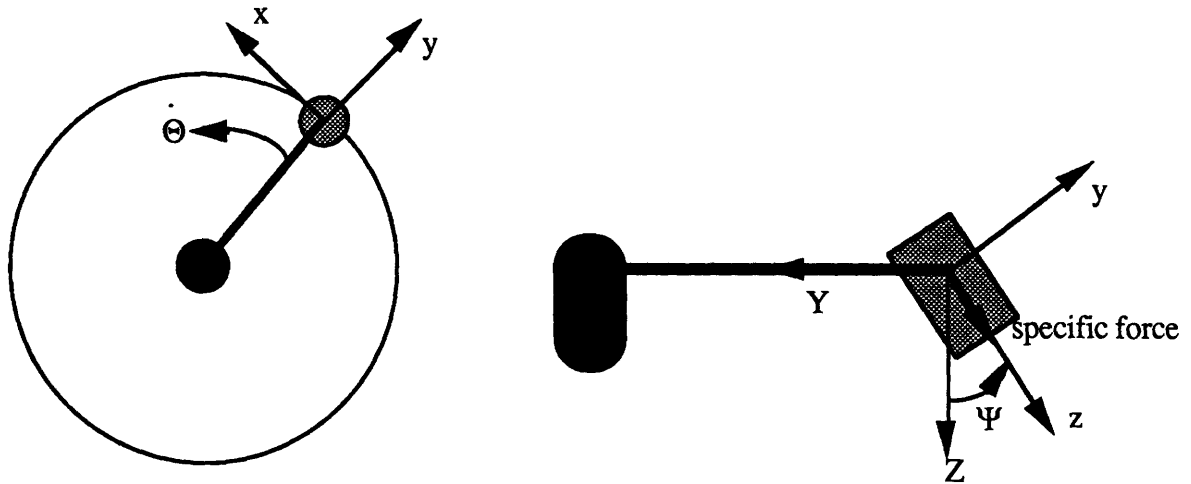


Figure 5.22 Model of a Centrifuge

With this simplified dynamics, we end up getting for the linear acceleration of the subject:

$$A = \dot{\Theta} \times r + \dot{\Theta} \times (\dot{\Theta} \times r) \text{ with } \dot{\Theta} = \begin{bmatrix} 0 \\ 0 \\ \dot{\Theta} \end{bmatrix}$$

Also, we get that:

$$\tan(\Psi) = -\frac{r \cdot \dot{\Theta}^2}{g} \text{ or } \Psi = \tan^{-1}\left(-\frac{r \cdot \dot{\Theta}^2}{g}\right)$$

and

$$\text{angvel} = \begin{bmatrix} \dot{\Psi} \\ 0 \\ \dot{\Theta} \end{bmatrix}_{X,Y,Z} = \begin{bmatrix} \dot{\Psi} \\ \dot{\Theta} \cdot \sin(\Psi) \\ \dot{\Theta} \cdot \cos(\Psi) \end{bmatrix}_{x,y,z}$$

$$\text{linacc} = A = -r \cdot \ddot{\Theta} X - r \cdot \dot{\Theta}^2 \cdot Y = -r \cdot \ddot{\Theta} \cdot x - r \cdot \dot{\Theta}^2 (\cos \Psi \cdot y - \sin \Psi \cdot z)$$

or

$$\text{linacc} = \begin{bmatrix} -r \cdot \ddot{\Theta} \\ -r \cdot \dot{\Theta}^2 \cdot \cos \Psi \\ r \cdot \dot{\Theta}^2 \cdot \sin \Psi \end{bmatrix}_{x,y,z}$$

With our conventions, a rotation where the subject faces the movement implies:

$$\dot{\Theta} \leq 0 \text{ and } \dot{\Psi} \leq 0$$

5.5.1 Stimulus to the Vestibular System

The following figures are showing the actual stimulus to the vestibular system, expressed in head coordinates, during a centrifuge experiment. The data are taken from the M.S. Thesis of Braden McGrath of the Man Vehicle Lab at MIT [24].

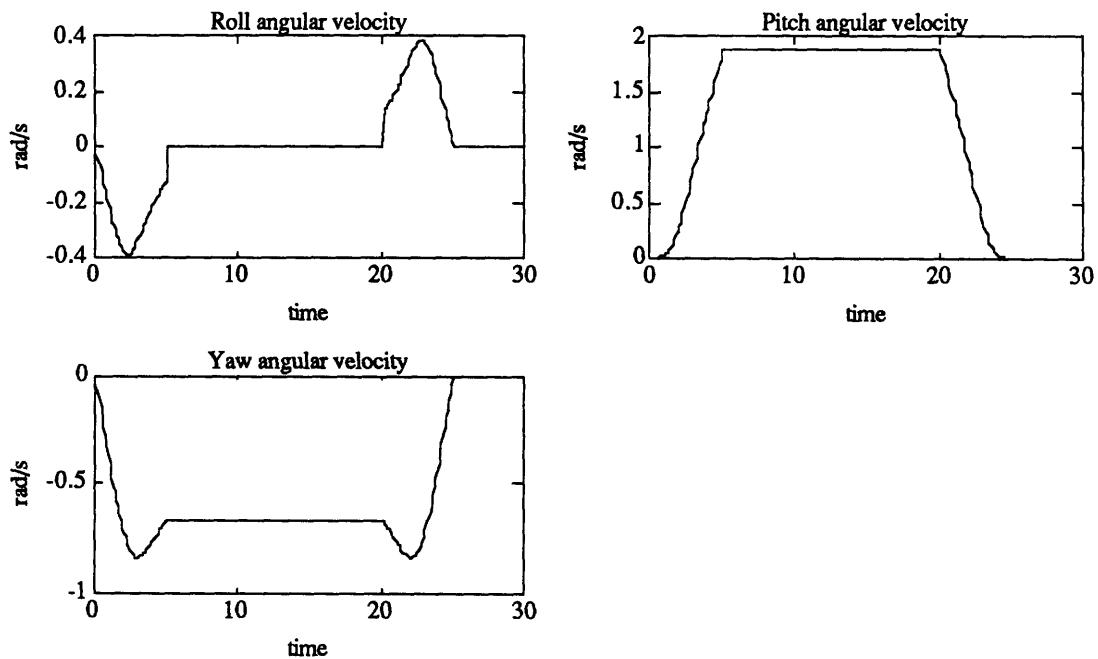


Figure 5.23 Angular Velocity Stimulus

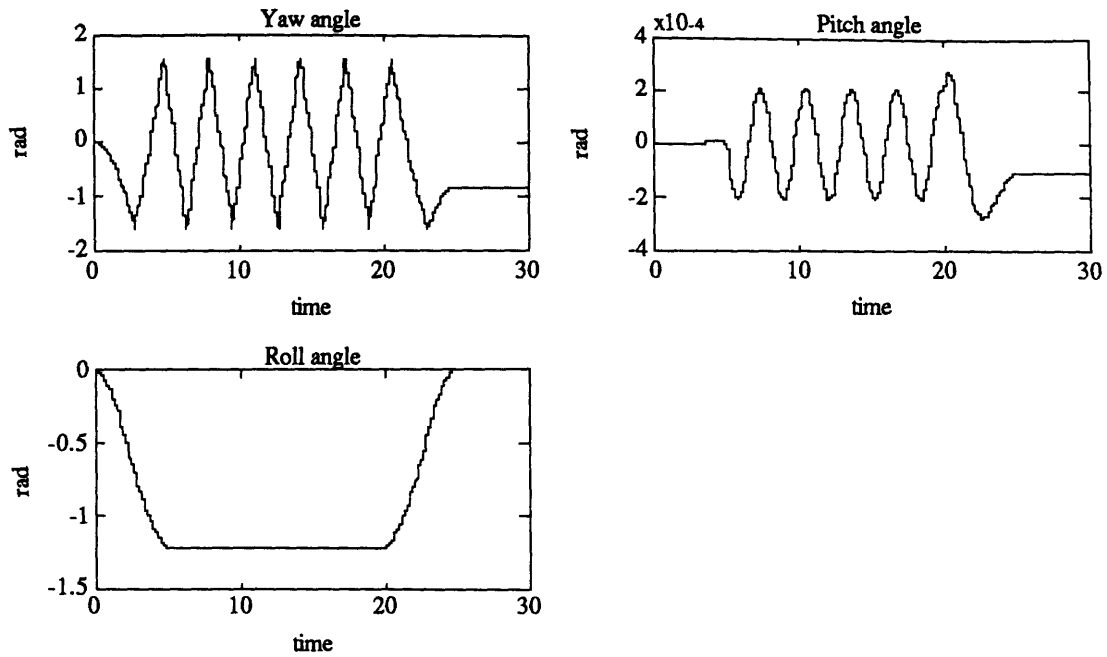


Figure 5.24 Orientation Angles

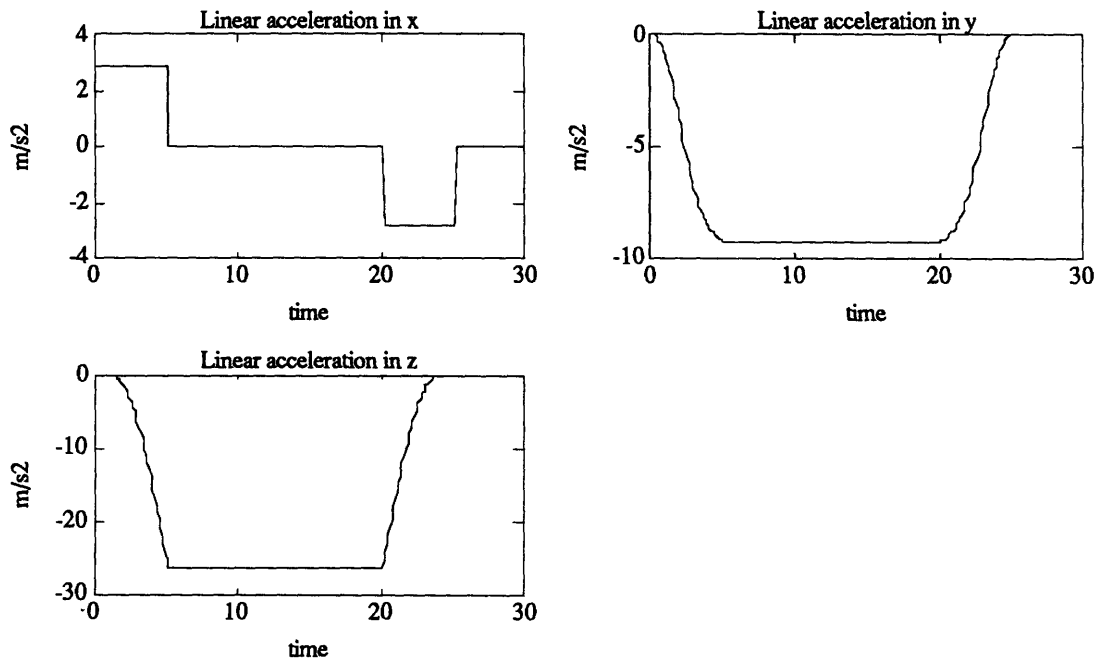


Figure 5.24 Linear Acceleration Stimulus

5.5.2 Simulation Results

The angular velocities, Euler angles and linear acceleration are estimated as follows:

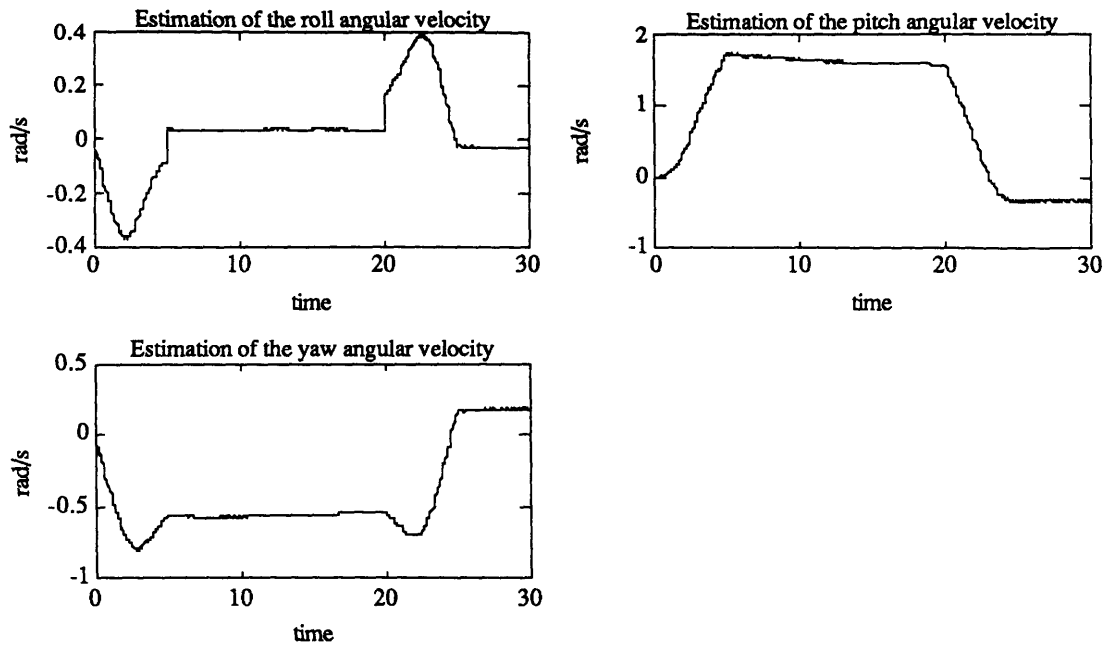


Figure 5.24 Estimation of the Angular Velocities

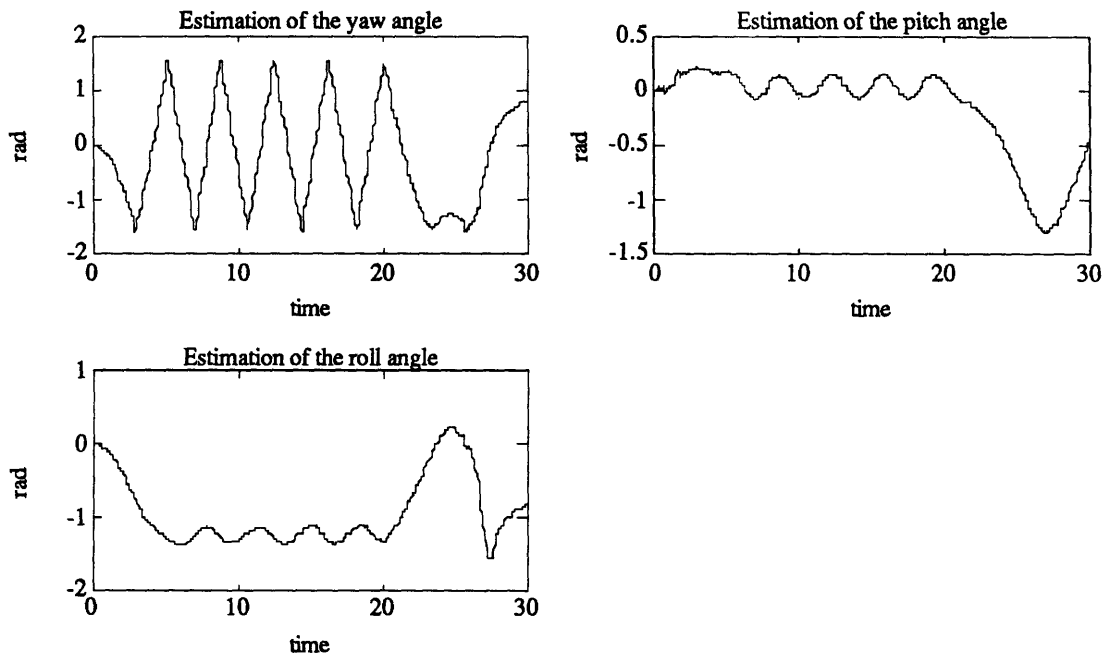


Figure 5.26 Estimation of the Euler Angles

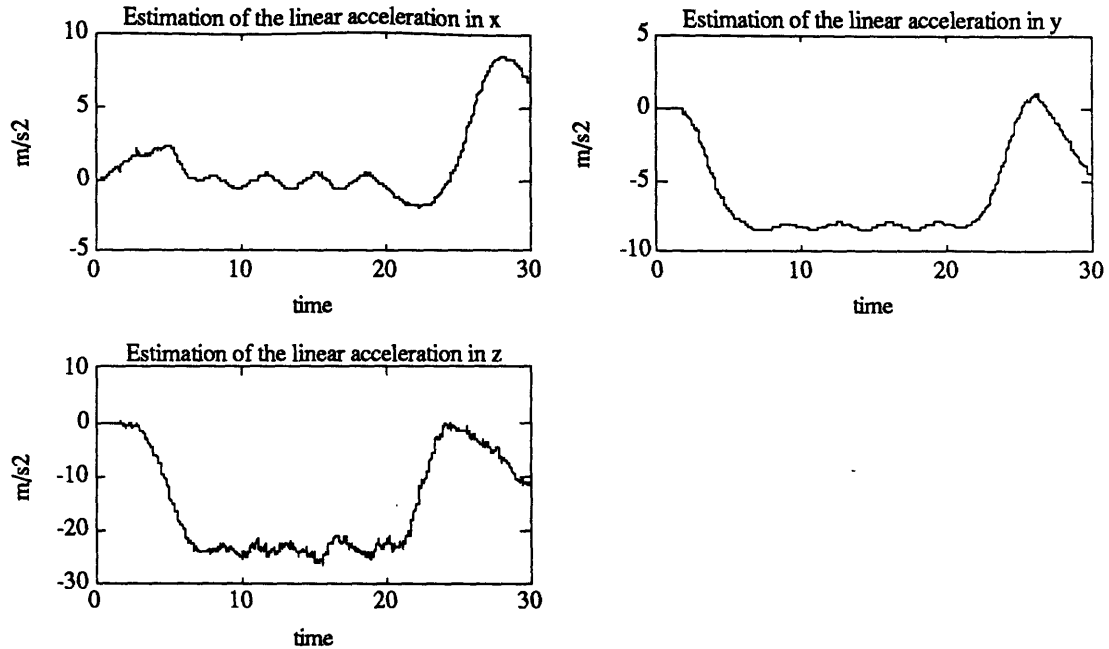


Figure 5.27 Estimation of the Linear Acceleration

Those results deserve a few comments. First, the calculation of the Euler angles from the quaternion vector, as explained in Appendix A, is valid for angles that are between $-\pi/2$ and $\pi/2$. In our case, the yaw angle is increasing at a rate of 2 rad/s when the centrifuge is stabilized, meaning that it goes above $\pi/2$ very quickly. In other words, the angle plotted in Figure 5.26 is the angle between $-\pi/2$ and $\pi/2$ that has the same sine as the yaw angle. A way to figure out the real yaw angle is to look at the yaw velocity. As this one is negative during most of the simulation time, the yaw angle is decreasing.

We can see that the roll angle is quite well estimated, meaning that the CNS kept track of the position of the gravity.

After the deceleration, we see that the estimated pitch angle decreases rapidly, giving an impression of tumbling around. Also, a strong forward linear acceleration is experienced after the centrifuge has stopped. All those phenomena are actually experienced by subjects in centrifuge experiments [24].

We see that the internal representation of the state variables that involve the quaternion vector (quaternion itself and linear movement) present oscillations. We didn't have the material to figure out whether it is coming from numerical errors (essentially from the quaternion), or if it corresponds to realistic sensations. This point needs to be investigated further.

Finally, due to memory limitations, we couldn't test our model on longer simulations. Comparison with real cases would need to run simulations for several minutes.

Chapter 6

Conclusions and Possible Improvements

6.1 Results Summary

Our model for the spatial orientation of a human using only the vestibular cues, has been tested on the generic cases used in previous major studies in the field (principally Borah et al [10]). Using a time-varying nonlinear filter model turned out to give as good or better results in any simulation cases. In particular, we solved some of the problems that Borah et al have pointed out:

(i) No large angle problems with the use of a quaternion integration in the internal model.

(ii) The linear velocity in the dark is correctly estimated as the integral of the estimated linear acceleration. Borah et al predicted an aberrant linear velocity with their model.

(iii) The pitch angle is correctly estimated in pitch simulation cases. The illusion of linear acceleration remains very small in the “in the dark” case, whereas Borah et al estimated an unrealistically large linear acceleration.

However, the simulations done on vection phenomena do not show the delays that are found in real experiments. Further modeling is then necessary, as discussed in the following paragraph.

6.2 Possible Improvements

The model that we developed used only vestibular cues to calculate the estimate of the spatial orientation state vector, whereas it is known, as described in Chapter 2, that other cues such as tactile or proprioceptive, play an important role in the orientation process. However, non-vestibular afferences are far less investigated in the literature than vestibular. It was then not worthwhile to add them, knowing that the added information would either degrade or

improve the estimate in an unrealistic way. Borah et al add to their model -as presented in Chapter 3- nonvestibular cues, but the results of their simulations turned out to be inconclusive. More experiments and modeling have to be done before including nonvestibular cues in a spatial orientation model.

A great deal of work, also, could be done by adding to the internal model, physiological parameters coming from “motion sickness” behavior involved in spatial orientation (or disorientation). The “measurement error” vector that is used in the Kalman Filter is called by Oman [12,13] the “sensory conflict” vector, and motion sickness phenomena can be affected by it, and influence it through internal feedback.

Actually, Oman showed that the physiological troubles that are associated with motion sickness can be modeled by dynamic systems driven by the “sensory conflict” vector. As the CNS is part of a body that is going to react to motion sickness, we can think that the orientation process might be affected. We know that pilots who are submitted to heavy workload have problems to accomplish simple tasks. Motion sickness adds workload on the CNS, and the orientation task can be affected adversely.

The observer gain could then be “scheduled” with respect to this “sensory conflict” vector, using adaptive filtering techniques. We believe, for example, that vection delays could be predicted with such techniques. More work along these lines needs to be carried out.

References

1. Freeman J. Personal letter from Air Force Inspection and safety Center to W.B. Alberty re: Low-altitude Class A Mishaps, dtd 10 March 89.
2. Marlowe B., "Spatial Disorientation and Loss of Attitude Awareness: Impact on the USAF". Presented at the 58th Annual Scientific Meeting of the Aerospace Medicine Association, May 10-14, 1987, Las Vegas.
3. Kirkham, W.R., et al, "Spatial Disorientation in General Aviation Accidents". Aviation Space and Environmental Medicine Med 49:1080-1086, 1978.
4. Gillingham K.K., "Spatial Disorientation Research at USAFAM". Presented at the 61st Annual Scientific Meeting of the Aerospace Medicine Association, May 13-17, 1990, New Orleans, Marriot Hotel.
5. Lyons T.J. and J.E. Freeman, "Spatial Disorientation Mishaps in the US Air Force in 1988". Presented at the 61st Annual Scientific Meeting of the Aerospace Medicine Association, May 13-17, 1990, New Orleans, Marriot Hotel.
6. Gillingham K.K. and J.W. Wolfe, "Spatial Orientation in Flight". USAF School of Aerospace Medicine, AFSC, USAFSAM-TR-85-31, December 1986.
7. Liebowitz H.W. and J. Dichgans, "The Ambient Visual System and Spatial Orientation". Spatial Disorientation in Flight: Current Problems. AGARD-CP-287. NATO/AGARD, Neuilly-sur-Seine, France, 1980.
8. Barson A.J. and S.F. Brown, "Thresholds for the Perception of Whole Body Angular Movement About the Vertical Axis". Aviation Space and Environmental Medicine, March, 1989.
9. Teas D.C., W.R. Ercoline, T.J. Lyons, K.K. Gillingham, "The Discriminability of Aircraft State Mediated by Acoustic Cues". Presented at the 61st Annual Scientific Meeting of the Aerospace Medicine Association, May 13-17, 1990, New Orleans, Marriot Hotel.

10. Borah J., L.R. Young, R.E. Curry, "Optimal Estimator Model for Human Spatial Orientation". Representation of Three-Dimensional Space in the Vestibular, Oculomotor, and Visual System: A Symposium of the Barany Society. Annals of the New York Academy of Sciences, Volume 545, New York, NY, 1988, pages 51-73.
11. Kalman, R.E. and R.S. Bucy, "New Results in Linear Filtering and Prediction Theory". J. Basic Eng. Trans. ASME Ser D 83:95-108, 1961.
12. Oman, C.M., "A Heuristic Mathematical Model for the Dynamics of Sensory Conflict and Motion Sickness". Acta Oto. Suppl. 392, 1982.
13. Oman, C.M., "Sensory Conflict and Motion Sickness: An Observer Theory Approach". Presented at the Symposium and Workshop on Spatial Displays and Spatial Instruments. Asilomar Ca., September 1988.
14. Young, L.R. and J.L. Meiry, "A Revised Dynamics Otolith Model". Aerosp. Med. 39: 606-608, 1968.
15. Young, L.R., "Visually Induced Motion In Flight Simulation". Advisory Group for Aeronautical Research and Dev. Conf. Proc.249: 16-1 to 16-8, 1978.
16. Merfeld, D. M.. "Spatial Orientation in the Squirrel Monkey: An Experimental and Theoretical Investigation". PhD Thesis, Department of Aeronautics and Astronautics, Man Vehicle Laboratory, January 1990.
17. Gum, D.R., "Modeling of the Human Force and Motion-sensing Mechanisms". AFHRL-TR-72-54, AD-766-444. 1973, Wright-Patterson Air Force Base, OH.
18. Young, L.R.. "On Visual Vestibular Interactions". Proc. 5th Symposium of the Role of the Vestibular Organs in Space Exploration. NASA SP 314:205-210.
19. Battin, R.H., An Introduction to the Mathematics and Methods of Astrodynamics, AIAA Education Series, 1987.
20. Gelb, A., and the Technical Staff of The Analytic Science Corporation. Applied Optimal Estimation. The MIT Press, 1974.

21. Grant, W., W. Best, "Otolith-Organ Mechanics: Lumped Parameter Model and Dynamics Response". Aviation Space and Environmental Medicine, October 1987.
22. Wolfe, J.W., R.L. Kramer, "Illusion of Pitch Induced by Centripetal Acceleration". Aerospace Medicine, 41(10): 1136-1139, 1970.
23. Chu, W., "Dynamics Response of Human Linearvection". S.M. Thesis, Department of Aeronautics and Astronautics, MIT, 1976.
24. McGrath, B. J., "Human Vestibular Response in 3 g's Centrifugation", S.M. Thesis, Department of Aeronautics and Astronautics, MIT, 1990.
25. Radix, J.C., Systèmes Inertiels. à Composants Liés "Strap-Down", Presses de l'ENSTA, 1984.

Appendix A

A.1 Calculation of the Euler angles

From the quaternions that were considered as part of the state vector, we have calculated the transformation matrix between the moving and the inertial coordinates:

$$\dot{q} = \frac{1}{2} \begin{bmatrix} 0 & -\omega_1 & -\omega_2 & -\omega_3 \\ \omega_1 & 0 & \omega_3 & -\omega_2 \\ \omega_2 & -\omega_3 & 0 & \omega_1 \\ \omega_3 & \omega_2 & -\omega_1 & 0 \end{bmatrix} q \quad q = \begin{bmatrix} q_0 \\ q_1 \\ q_2 \\ q_3 \end{bmatrix}$$

$$B = \begin{bmatrix} q_0^2 + q_1^2 - q_2^2 - q_3^2 & 2(q_1q_2 - q_0q_3) & 2(q_1q_3 + q_0q_2) \\ 2(q_1q_2 + q_0q_3) & q_0^2 + q_2^2 - q_1^2 - q_3^2 & 2(q_3q_2 - q_0q_1) \\ 2(q_1q_3 - q_0q_2) & 2(q_2q_3 + q_0q_1) & q_0^2 + q_3^2 - q_1^2 - q_2^2 \end{bmatrix}$$

If we now consider that this transformation matrix is the linear operator corresponding to the following transformation:

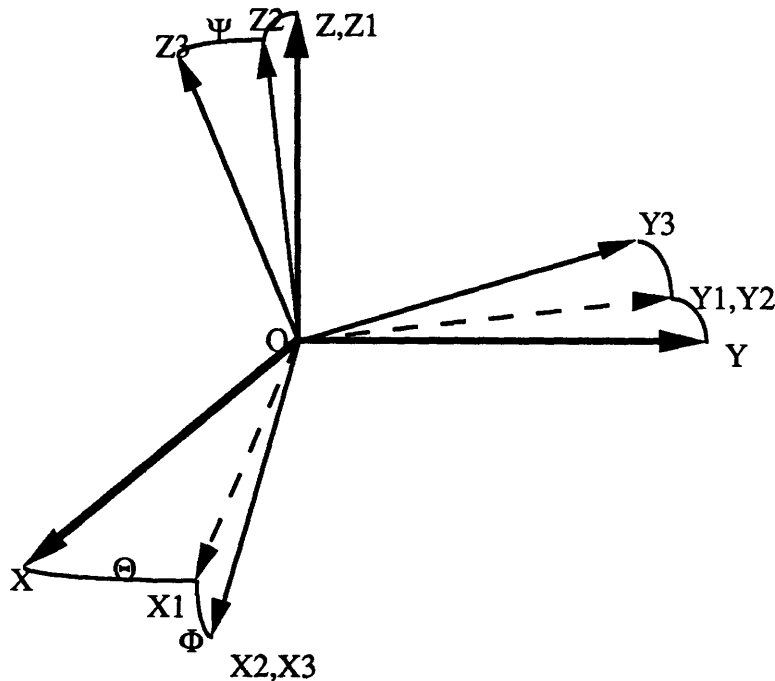


Figure A.1

where we have the succession of three rotations of angles Θ, Φ, Ψ and about Z, Y1 and X2 respectively, we can derive that:

$$B = \begin{bmatrix} \cos \Phi \cdot \cos \Theta & -\sin \Theta \cos \Phi + \cos \Theta \sin \Phi \sin \Psi & \sin \Theta \sin \Psi + \cos \Theta \sin \Phi \cos \Psi \\ \cos \Phi \cdot \sin \Theta & \cos \Psi \cdot \cos \Theta + \sin \Theta \sin \Phi \sin \Psi & -\sin \Psi \cdot \cos \Theta + \sin \Theta \sin \Phi \cos \Psi \\ -\sin \Phi & \sin \Psi \cdot \cos \Phi & \cos \Psi \cdot \cos \Phi \end{bmatrix}$$

Knowing the matrix $B=b(i,j)$, we can easily calculate the angles Θ, Φ, Ψ , when their values are between $-\pi/2$ and $+\pi/2$.

$$\Theta = \sin^{-1} \left(\frac{b(2,1)}{\cos(\Phi)} \right)$$

$$\Phi = \sin^{-1}(b(3,1))$$

$$\Psi = \sin^{-1} \left(\frac{b(3,2)}{\cos(\Phi)} \right)$$

As the terms $b_{i,j}$ can directly be expressed in terms of the state vector, those equations can be implemented as measurement equations in the Extended Filter. This measurement corresponds to the interpretation of the instrument panel by the pilot, or to a look outside of the cockpit. Φ and Ψ are given by the artificial horizon, Θ by the ball.

Appendix B

B.1 Example of Quaternion Estimate

The following two figures show the differences on the norm of the quaternion vector, when using the Extended Kalman Filter with and without the nonlinear measurement on the norm.

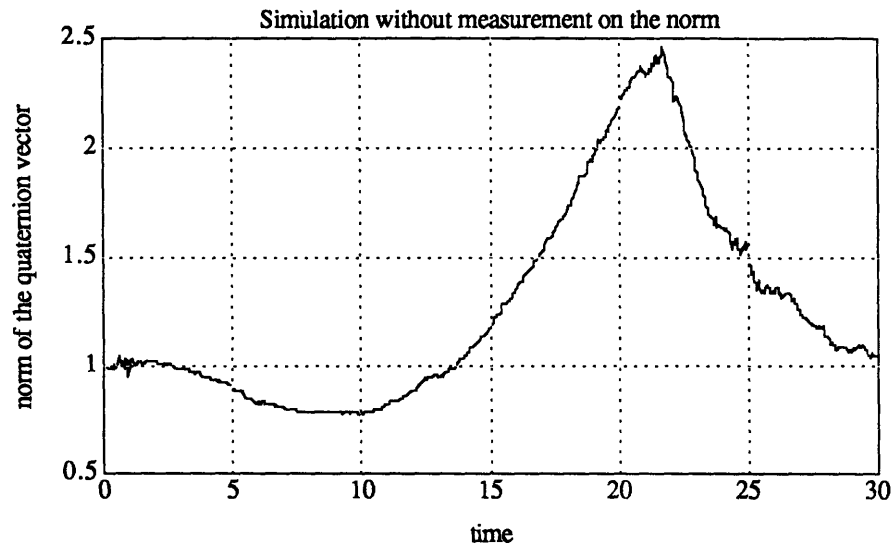


Figure B.1

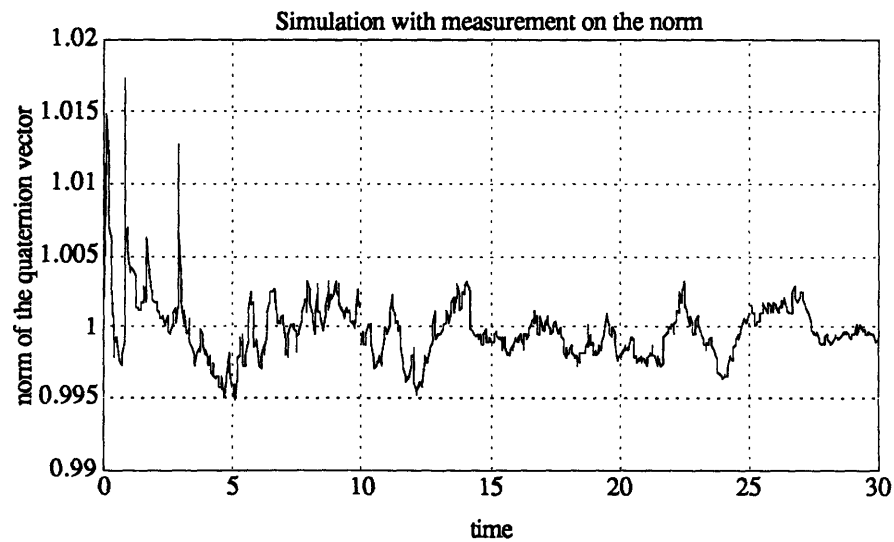


Figure B.2

Appendix C

C.1 Main MatLab Code

We are giving in this Appendix the Matlab code that we used for the simulations.

angvel(t) and **linacc(t)** are two small functions that calculate the angular velocities and the linear acceleration as a function of time.

```
function y=angvel(t)
if t<=1
y(3)=.26*t;
else
y(3)=.26;
end
y(1:2)=zeros(1,2);
```

```
function y=linacc(t)
if t<=3
y(1)=30;
else
y(1)=0;
end
y(2:3)=zeros(1,2);
```

thmodel(t,x) is the function that calculates the derivative of the “real” state vector in the Time History generation process.

```
function y=thmodel(t,X)

% Where dX/dt=thmodel(t,X)

% Generation of the input
```

```

u=angvel(t);
v=linacc(t);

% Head to otoliths change

c=cos(25*pi/180);
s=sin(25*pi/180);
B2=[c 0 -s;0 1 0;s 0 c];

% Head to canals coordinates

q=1/sqrt(2);
B1=B2*[q -q 0;q q 0;0 0 1];

% Quaternion integration

N=sqrt(X(1)^2+X(2)^2+X(3)^2+X(4)^2);
X(1)=X(1)/N;
X(2)=X(2)/N;
X(3)=X(3)/N;
X(4)=X(4)/N;

y(1)=.5*(-u(1)*X(2)-u(2)*X(3)-u(3)*X(4));
y(2)=.5*(u(1)*X(1)+u(3)*X(3)-u(2)*X(4));
y(3)=.5*(u(2)*X(1)-u(3)*X(2)+u(1)*X(4));
y(4)=.5*(u(3)*X(1)+u(2)*X(2)-u(1)*X(3));

B(1,1)=X(1)^2+X(2)^2-X(3)^2-X(4)^2;
B(2,1)=2*(X(2)*X(3)+X(1)*X(4));
B(3,1)=2*(X(2)*X(4)-X(1)*X(3));
B(1,2)=2*(X(2)*X(3)-X(1)*X(4));
B(2,2)=X(1)^2+X(3)^2-X(2)^2-X(4)^2;
B(3,2)=2*(X(3)*X(4)+X(1)*X(2));
B(1,3)=2*(X(2)*X(4)+X(1)*X(3));
B(2,3)=2*(X(4)*X(3)-X(1)*X(2));
B(3,3)=X(1)^2+X(4)^2-X(2)^2-X(3)^2;

% Angular velocity and angular acceleration

y(5)=0;
y(6)=0;
y(7)=0;

```

```
% Linear velocity and linear acceleration
```

```
y(8)=v(1);  
y(9)=v(2);  
y(10)=v(3);
```

```
y(11)=0;  
y(12)=0;  
y(13)=0;
```

```
% Semicircular canal response
```

```
u=B1*u';
```

```
y(14)=X(15);  
y(15)=-.002075*X(14)-.1792*X(15)+u(1);  
y(16)=X(17);  
y(17)=-.002075*X(16)-.1792*X(17)+u(2);  
y(18)=X(19);  
y(19)=-.002075*X(18)-.1792*X(19)+u(3);
```

```
% Otoliths response
```

```
sf=B'*[0;0;9.81]-v';
```

```
% transformation to otolith coordinates
```

```
sf1=B2*sf;
```

```
y(20)=X(21);  
y(21)=-10*X(20)-100.1*X(21)+sf1(1);  
y(22)=X(23);  
y(23)=-10*X(22)-100.1*X(23)+sf1(2);  
y(24)=X(25);  
y(25)=-10*X(24)-100.1*X(25)+sf1(3);
```

```
y=y';
```

RK3(function,h,t0,tf,x) integrates the function from t0 to tf, with initial condition x, and using a Runge-Kutta of the third order.

```

function [t,y]=RK3 (FunFcn,h,to,tf,x)

y=x;
t=to;

while to<tf
    s1=feval (FunFcn,to,x) ;
    s2=feval (FunFcn,to,x+h*s1) ;
    s3=feval (FunFcn,to+h/2,x+h*(s1+s2)/4) ;

    x=x+h*(s1+s2+4*s3)/6;
    to=to+h;
    y=[y,x];
    t=[t,to];
end

```

AFR(x,u,v,TH,THs,sat,B1,B2) calculate the afferent firing rates of the internal sensors, from the state vector x , the angular velocities u , the linear acceleration v , the thresholds and saturations (TH , THs , sat) and the transformation matrices from the head coordinates to the canal and otolith coordinates, respectively ($B1$, $B2$).

```

function y=AFR(X,u,v,TH,THs,sat,B1,B2) ;

% Semicircular canals afference

u1=B1*u';

y(1)=-0.0021*X(14)-.1792*X(15)+u1(1) ;
y(2)=-0.0021*X(16)-.1792*X(17)+u1(2) ;
y(3)=-0.0021*X(18)-.1792*X(19)+u1(3) ;

y(1)=thres (y(1),TH(1)) ;
y(2)=thres (y(2),TH(2)) ;
y(3)=thres (y(3),TH(3)) ;

y(1:3)=(B1'*y(1:3))' ;

```

```

% Circular vection

y(4)=satur(u(1),THs(1),sat(1));
y(5)=satur(u(2),THs(2),sat(2));
y(6)=satur(u(3),THs(3),sat(3));

% Focal vision

%y(13)=asin(2*(X(2)*X(4)-X(1)*X(3)));
%y(14)=asin(2*(X(2)*X(3)+X(1)*X(4))/sqrt(1-
4*(X(2)*X(4)-X(1)*X(3))^2));
%y(15)=asin(2*(X(3)*X(4)+X(1)*X(2))/sqrt(1-
4*(X(2)*X(4)-X(1)*X(3))^2));

% Linear vection

y(7)=satur(X(8),THs(4),sat(4));
y(8)=satur(X(9),THs(5),sat(5));
y(9)=satur(X(10),THs(6),sat(6));

% Otolith afference

y(10)=thres(X(20),TH(4));
y(11)=thres(X(22),TH(5));
y(12)=thres(X(24),TH(6));

y(10:12)=(B2'*y(10:12)')';

y=y';

```

thgeneration initializes the simulation and integrates **thmodel** to generate the set of corresponding measurements.

```

clear
rand('normal')

% Calculation of the measurement vector, or Time
History Generation

```

```

% init of the state vector

x0=[1 0 0 0 0 0 0 0 0 0 0 0 0 0 0 0 0 0 0 0 0 0 -.41459 0 0
0 .88909 0]';

% generation of the set of measurements

% Values of the thresholds and saturations

% Semicircular canals

TH(1)=2;    % deg/s
TH(2)=2;
TH(3)=2;

% Otoliths

TH(4)=0.063;    % m/s2
TH(5)=0.057;
TH(6)=0.154;

% Saturations

sat (1)=60*pi/180;    % rad/s
sat (2)=60*pi/180;
sat (3)=60*pi/180;

sat (4)=100;    % m/s
sat (5)=100;
sat (6)=100;

% Thresholds for the vection

THs=zeros (1,6);

% COORDINATE MATRICES

% Head to otoliths change

c=cos (25*pi/180);
s=sin (25*pi/180);
B2=[c 0 -s;0 1 0;s 0 c];

```

```

% Head to canals coordinates

q=1/sqrt(2);
B1=B2*[q -q 0;q q 0;0 0 1];

% Beginning and end of the simulation

t0=0;    % sec
tf=30;
h=.01;

% Simulation using Runge-Kutta 2nd and 3rd order

[t,x]=RK3('thmodel',h,t0,tf,x0);

% Calculation of the afferent firing rates

k=length(t);
for i=1:k
    u=angvel(t);
    v=linacc(t);
    z(:,i)=AFR(x(:,i),u,v,TH,THs,sat,B1,B2);
end

% z contains the measurement values

```

model(t,x,br,bl) calculates the derivative of the estimated state based on the internal model. The values of the expected frequency bandwidth are entered as parameters (br,bl).

```

function y=model(X,br,bl)

% Where  $\frac{dX}{dt}=\text{model}(X)$ 

% Generation of the input

% Quaternion integration

```

```

y(1)=.5*(-X(5)*X(2)-X(6)*X(3)-X(7)*X(4));
y(2)=.5*(X(5)*X(1)+X(7)*X(3)-X(6)*X(4));
y(3)=.5*(X(6)*X(1)-X(7)*X(2)+X(5)*X(4));
y(4)=.5*(X(7)*X(1)+X(6)*X(2)-X(5)*X(3));

```

```

B(1,1)=X(1)^2+X(2)^2-X(3)^2-X(4)^2;
B(2,1)=2*(X(2)*X(3)+X(1)*X(4));
B(3,1)=2*(X(2)*X(4)-X(1)*X(3));
B(1,2)=2*(X(2)*X(3)-X(1)*X(4));
B(2,2)=X(1)^2+X(3)^2-X(2)^2-X(4)^2;
B(3,2)=2*(X(3)*X(4)+X(1)*X(2));
B(1,3)=2*(X(2)*X(4)+X(1)*X(3));
B(2,3)=2*(X(4)*X(3)-X(1)*X(2));
B(3,3)=X(1)^2+X(4)^2-X(2)^2-X(3)^2;

```

% Angular velocity and angular acceleration

```

y(5)=-br*X(5);
y(6)=-br*X(6);
y(7)=-br*X(7);

```

% Linear velocity and linear acceleration

```

y(8)=X(11);
y(9)=X(12);
y(10)=X(13);

```

```

y(11)=-bl*X(11);
y(12)=-bl*X(12);
y(13)=-bl*X(13);

```

% Semicircular canal response

```

y(14)=X(15);
y(15)=-.002075*X(14)-.1792*X(15)+X(5);
y(16)=X(17);
y(17)=-.002075*X(16)-.1792*X(17)+X(6);
y(18)=X(19);
y(19)=-.002075*X(18)-.1792*X(19)+X(7);

```

% Otoliths response

```

sf=B'*[0;0;9.81]-X(11:13);

```

```

y(20)=X(21);
y(21)=-10*X(20)-100.1*X(21)+sf(1);
y(22)=X(23);
y(23)=-10*X(22)-100.1*X(23)+sf(2);
y(24)=X(25);
y(25)=-10*X(24)-100.1*X(25)+sf(3);

```

```

y=y'; % column vector

```

grad(x) calculates the gradient matrix in x, of the internal representation of the dynamic function.

```

function y=grad(x,br,bl)

g=9.81;

% This function calculate the gradient in x of the
% internal model function

y(1,:)= [0 -.5*x(5) -.5*x(6) -.5*x(7) -.5*x(2) -.5*x(3)
-.5*x(4) zeros(1,18)];
y(2,:)= [.5*x(5) 0 .5*x(7) -.5*x(6) .5*x(1) -.5*x(4)
.5*x(3) zeros(1,18)];
y(3,:)= [.5*x(6) -.5*x(7) 0 .5*x(5) .5*x(4) .5*x(1) -
.5*x(2) zeros(1,18)];
y(4,:)= [.5*x(7) .5*x(6) -.5*x(5) 0 -.5*x(3) .5*x(2)
.5*x(1) zeros(1,18)];

y(5:7,1:25)=[zeros(3,4) -br*eye(3) zeros(3,18)];

y(8:10,1:25)=[zeros(3,10) eye(3) zeros(3,12)];

y(11:13,1:25)=[zeros(3,10) -bl*eye(3) zeros(3,12)];

y(14:15,1:25)=[zeros(2,4) [0;1] zeros(2,8) [0 1;-
.002075 -.1792] zeros(2,10)];

y(16:17,1:25)=[zeros(2,5) [0;1] zeros(2,9) [0 1;-
.002075 -.1792] zeros(2,8)];

```

```

y(18:19,1:25)=[zeros(2,6) [0;1] zeros(2,10) [0 1;-
.002705 -.1792] zeros(2,6)];

y(20,:)=[zeros(1,19) 0 1 0 0 0 0];
y(21,:)=[-2*g*x(3),2*g*x(4),-
2*g*x(1),2*g*x(2),zeros(1,6),-1 0 0,zeros(1,6),-10 -
100.1 0 0 0 0];

y(22,:)=[zeros(1,19) 0 0 0 1 0 0];
y(23,:)=[2*g*x(2),2*g*x(1),2*g*x(4),2*g*x(3),zeros(1,6
),0 -1 0,zeros(1,6),0 0 -10 -100.1 0 0];

y(24,:)=[zeros(1,19) 0 0 0 0 0 1];
y(25,:)=[2*g*x(1),-2*g*x(2),-
2*g*x(3),2*g*x(4),zeros(1,6),0 0 -1,zeros(1,6),0 0 0 0
-10 -100.1];

```

meas(x) calculates the expected measurement from the estimated state vector. The measurement vector is given “in the dark”, meaning without visual cues.

```

function y=meas(x)

y(1)=x(1)^2+x(2)^2+x(3)^2+x(4)^2;

% measurement matrix

A=[-.0021 -.1792 0 0 0 0;0 0 -.0021 -.1792 0 0;0 0 0 0
-.0021 -.1792];
B=[1 0 0 0 0 0;0 0 1 0 0 0;0 0 0 0 1 0];
H=[zeros(3,4) eye(3) zeros(3,6) A zeros(3,6)
zeros(3,19) B];

y(2:7)=H*x;

y=y';

```

gmeas(x) calculates the gradient in x , of the measurement equation in the dark.

```
function H=gmeas(x)

H(1,:)= [2*x(1) 2*x(2) 2*x(3) 2*x(4) zeros(1,21)];

A=[-.0021 -.1792 0 0 0 0;0 0 -.0021 -.1792 0 0;0 0 0 0
-.0021 -.1792];
B=[1 0 0 0 0 0;0 0 1 0 0 0;0 0 0 0 1 0];
H(2:7,:)= [zeros(3,4) eye(3) zeros(3,6) A zeros(3,6)
zeros(3,19) B];
```

filter(t,z) initializes the Extended Kalman Filter and uses the set of measurements to calculate the estimate of the state vector. $t=[t_0:timestep:tf]$, and z is a vector containing the measurements taken at each time step.

```
% initialisation

xe=[1 0 0 0 0 0 0 0 0 0 0 0 0 0 0 0 0 0 0 0 0 .981
0]';
xhat=xe;

% initial covariance

P=diag([.01*ones(1,10) .1*ones(1,3) .01*ones(1,12)]);

% covariance of the driving noise

Q=[zeros(4,25);
zeros(3,4) eye(3) zeros(3,18);
zeros(3,25);
zeros(3,10) 10*eye(3) zeros(3,12);
zeros(12,25)];

R=diag([.0001, .0001, .0001, .0001, .001, .001, .001]);
```

```

ro=sqrt(R);

% Parameters of the internal model

br=10;
bl=.1;
h=.01;

% Filtering equation

for i=1:(length(t)-1)/4

k=4*i;

    for j=1:4

% Propagation of the estimate using Runge Kutta

s01=model(xe,br,bl);
s02=grad(xe,br,bl)*P+P*grad(xe,br,bl)'+Q;

xe1=xe+h*s01;
P1=P+h*s02;

s11=model(xe1,br,bl);
s12=grad(xe1,br,bl)*P1+P1*grad(xe1,br,bl)'+Q;

xe2=xe+h*(s01+s11)/4;
P2=P+h*(s02+s12)/4;

s21=model(xe2,br,bl);
s22=grad(xe2,br,bl)*P2+P2*grad(xe2,br,bl)'+Q;

xe=xe+h*(s01+s11+4*s21)/6;
P=P+h*(s02+s12+4*s22)/6;

    end

% Covariance of the output & measurement noise

y=z(:,k);
r=diag(ro*y);

```

```

% Kalman gain and covariance update

H=gmeas(xe);
K=P*H'/(H*P*H'+R);
P=(eye(25)-K*H)*P*(eye(25)-K*H)'+K*R*K';

% Noisy measurement and estimate update

y=y+r*rand(7,1);
xe=xe+K*(y-meas(xe));

xhat=[xhat,xe];

end

```

C.2 Mechanism of a Simulation

A simulation starts with the definition of the angular velocities and linear acceleration.

Then run **thgeneration** after having set the parameters (initial time, final time, thresholds and so on).

Finally run **filter**. The estimate of the state vector is stored in the columns of the variable **xhat**.